## DISCLAIMER

This document was prepared as an account of work sponsored by the United States Government. While this document is believed to contain correct information, neither the United States Government nor any agency thereof, nor the Regents of the University of California, nor any of their employees, makes any warranty, express or implied, or assumes any legal responsibility for the accuracy, completeness, or usefulness of any information, apparatus, product, or process disclosed, or represents that its use would not infringe privately owned rights. Reference herein to any specific commercial product, process, or service by its trade name, trademark, manufacturer, or otherwise, does not necessarily constitute or imply its endorsement, recommendation, or favoring by the United States Government or any agency thereof, or the Regents of the University of California. The views and opinions of authors expressed herein do not necessarily state or reflect those of the United States Government or any agency thereof or the Regents of the University of California.

UCRL-19428

c. 2 Repl.

RECEIVED
LAWRENCE
BERKELEY LABORATORY

FEB 6 1979

LIBRARY AND
DOCUMENTS SECTION

# STOPPING POWER AND RANGE FOR ANY NUCLEUS IN ANY NONGASEOUS MATERIAL -- A COMPOSITE METHOD*

Palmer G. Steward† and Roger W. Wallace

Lawrence Radiation Laboratory
University of California
Berkeley, California 94720

September 1970

*Work done under auspices of the U.S. Atomic Energy Commission.

†Present address: Department of Radiology, Stanford University School of Medicine, Stanford, CA 94305.

UCRL-19428
c. 2 Repl.

# 1. INTRODUCTION

The purpose of the research reported here is to provide estimates of the stopping power and range of any atomic nucleus moving in any stopping medium. The range of kinetic energies considered varies from 10 to 1 000 MeV/amu.

The applications of these data fall into two main categories. First, when the charged particles are themselves incident upon the target material, as in irradiation with a monoenergetic beam from a particle accelerator, stopping power is basic to the calculation of important beam parameters. Such parameters include dose, particle energy spectrum, LET spectrum, and beam width, all as a function of depth in the tissue. These calculations have been performed for a variety of target materials, including water, by Litton, Lyman, and Tobias (1968) and Litton (1967) by introducing the effects of straggling, removal of particles due to nuclear collisions, and multiple Coulomb scattering.

The second application of these data is to the calculation of energy deposition and ranges of heavy secondary particles. For example, in neutron irradiation, the entire dose is deposited by secondary particles. In $\pi^-$-meson irradiation, the high-LET dose deposited by star formation is due to these heavy secondaries. These stopping-power and range data are of general application to the analysis of experiments involving charged-particle accelerators, cosmic rays, or the fission process.

Throughout this paper we refer to MeV/amu, represented by the symbol $\varepsilon$, as a unit of specific energy. (See "Notations" in the Appendix.) It is a unit intermediate between velocity and energy.

The relationship to velocity is given by

$$\varepsilon = 931\left[(1-\beta^2)^{-1/2} - 1\right]$$

or

$$\beta = \frac{\frac{\varepsilon}{931}\left(\frac{\varepsilon}{931} + 2\right)^{1/2}}{\frac{\varepsilon}{931} + 1}$$

and the relationship to energy is given by $\varepsilon = E/A_1$. The slowing-down mechanism of a charged particle in matter is similar throughout any plane of constant velocity in $(V, Z_1, Z_2)$ space. Since $\varepsilon$ is a function of velocity only, the same statement can be made regarding any plane of constant specific energy in $(\varepsilon, Z_1, Z_2)$ space.

We will find it convenient in this report to discuss information in terms of $(\varepsilon, Z_1, Z_2)$ space. For instance, in fig. 1 the slabs covering the bottom and part of the back of the box represent the volume of this space for which present accelerators can provide heavy particles. Alpha particles, as indicated in the figure, can be accelerated to 230 MeV/amu. Protons, represented by the bottom slab, can be accelerated above 500 MeV/amu. The slab along the back of the box describes the capabilities of present heavy-ion accelerators. Throughout most of this discussion the boundaries of the space we consider are given by: $0.01 \leq \varepsilon \leq 500$, $1 \leq Z_1 \leq 92$, $1 \leq Z_2 \leq 92$. These boundaries are somewhat arbitrary, and have been set primarily for the purpose of drawing figures.

Using this $(\varepsilon, Z_1, Z_2)$ space as a device for restating the purpose of this research, we may say that is our aim in this report to provide a computational method for filling the box in fig. 1 with range

and stopping-power data. The range we calculate is the total path-length mean range and does not take into consideration the shortening of the projected range due to Coulomb multiple scattering.

The approximate limits of the only useful experimental stopping-power or range data available are illustrated in fig. 1. Northcliffe (1963) has produced the most useful summary of these data in the slab against the back of the box. Whaling (1958) has summaried the data in this slab extensively for protons and alpha particles and also for heavier ions in gases. The researchers who originally obtained these data are summarized by Hyde (1964) and Aras, Menon, and Gordon (1965). Experimental data in the two narrow slabs against the bottom of the box are of only minor concern to us here; theory can accurately calculate these values. Since the data from these small regions must be extrapolated throughout the entire volume of the box, it is clear that it is of primary importance to include enough physical theory to make this extrapolation effective.

## 1.1 Stopping-Power Theory

The interactions of energetic heavy charged particles with matter have been of great interest for more than half a century. Bohr (1913, 1915) developed the semiclassical stopping-power theory using impact parameters in 1913. Bethe (1930, 1932) published his purely quantum mechanical theory in 1930.

Each of those theories is valid in only part of the ( $\varepsilon$, $Z_1$, $Z_2$) space. Bohr's theory is valid only when the following inequalities are satisfied [Bohr (1948)]:

$$Z_2 \ll 137\,\beta, \tag{1}$$

$$(Z_2^2\, r Z_1)^{1/3} \ll 137\,\beta,$$

$$\frac{\hbar}{mV} \ll \text{screening distance of scattering atom, and}$$

$$r Z_1 \gg 137\,\beta, \tag{2}$$

where $\hbar$ is Plank's constant divided by $2\pi$, m is the mass of the ion, V is its velocity, and the screening distance of an atom is the distance from its nucleus to the radius where the screening by its electron cloud has reduced the effective nuclear charge to 1/e of its true value. (See the Appendix for notations.)

The expression 137 $\beta$ appears many times throughout this paper. This expression is the ion velocity in units of the Bohr orbital K-shell velocity of the hydrogen atom. In discussion of the interactions of charged particles with matter, this is a very convenient unit of velocity. Since the K-shell electron velocity of the one-electron atom is proportional to the charge of the nucleus, inequality (1) can be restated: "In order for Bohr's theory to be valid, the velocity of the ion must be greater than the K-shell electron velocity of the stopping medium." Similarly, inequality (2) limits the ion velocity to less than its own K-shell electron velocity. Therefore Bohr's theory is limited to that region of ($\varepsilon$, $Z_1$, $Z_2$) space where the ion carries along with it its own electron cloud. This limits the usefulness of Bohr's theory to the few cases for which adequate charge-state data are available.

Bethe's theory, because use was made of the Born approximation, is limited to the region where

$$rZ_1 \ll 137\,\beta\,, \tag{3}$$

However, it was shown later by Mott (1931) that the less restrictive inequality (3) or

$$rZ_1 \ll Z_2 \tag{4}$$

is sufficient. Thus, since the K-shell velocity of the ion is approximately $\beta = Z_1/137$, the use of Bethe's theory is essentially restricted to the region of ($\varepsilon$, $Z_1$, $Z_2$) space where the ion is completely ionized, although for very low energy, when $r \approx 0$, the theory is again valid. Bethe originally also required inequality (1). However, he later showed with Livingston how the inclusion of shell corrections could eliminate the need for this inequality (Livingston and Bethe 1937). These shell corrections, in effect, subtract from Bethe's formula the contribution to the stopping power of those most tightly bound electrons in the stopping medium, which, at low ion velocities, are rarely excited. Walske (1952) made a detailed derivation of the K-shell correction. He later made an estimate for the L shell correction (Walske 1956). Recently Bichsel (1961) has estimated corrections for all higher shells of the stopping atom.

In 1933 Bloch (1933) developed his theory which, in addition to inequality (1), is restricted by $(Z_2 r Z_1)^{1/2} \ll 137\,\beta$. Bloch's theory provides a bridge between Bethe's and Bohr's theories in the sense that Bloch's theory agrees with Bohr's theory in the limit of inequality (2) and with Bethe's theory in the limit of inequality (3).

Each of these theories gives the stopping power in the form

$$\frac{dE}{dR} = 0.3072 \frac{(rZ_1)^2}{\beta^2 A_2} B. \tag{5}$$

Bohr found

$$B = Z_2 \left[ \ln \frac{1.123\, m_e V^3}{rZ_1 e^2 \omega} - \ln(1-\beta^2) - \beta^2 \right],$$

where $\omega$ may be regarded as an effective oscillation frequency of the electrons in the scattering atom. For Bethe's theory, including shell corrections,

$$B = Z_2 \left[ \ln \frac{2m_e c^2 \beta^2}{I} - \ln(1-\beta^2) - \beta^2 - \frac{\sum_i C_i}{Z_2} - \delta \right]. \tag{6}$$

Here I is the average excitation potential of the stopping medium, $\sum_i C_i$ is the sum of the shell corrections summed over the electronic shells of the stopping medium (i.e., i = K, L, M, $\cdots$), and $\delta$ is the correction due to polarization of the stopping medium. For our purposes we may neglect $\delta$, since it makes a significant contribution only for ion specific energies above 500 MeV/amu. Even at 1000 MeV/amu, $\delta$ reduces the stopping power by less than 1%. For Bloch's theory

$$B = Z_2 \left[ \ln \frac{2m_e c^2 \beta^2}{I} + \psi(1) - \mathrm{Re}\,\psi \left[ 1 + i \frac{rZ_1}{137\beta} \right] - \ln(1-\beta^2) - \beta^2 \right],$$

where $\psi$ is the logarithmic derivative of the gamma function.

The usefulness of any of these theories is limited for $137\beta \leq Z_1$ because for these low velocities the ion carries along its own electron cloud, implying that r is less than 1 and is usually unknown. As stated

above, this makes Bohr's theory not generally useful, because his theory is valid only when this inequality holds. It also makes Bloch's theory not very useful except in the region of ( $\varepsilon$, $Z_1$, $Z_2$) space, where Bethe's theory is also valid. Lindhard and Scharff (1961) and Lindhard, Scharff, and Schiott (1963), hereafter referred to as LSS, have recently developed the only generally useful theory valid at low ion velocities. LSS have made use of the Thomas-Fermi description of the electron clouds of the ion and stopping atom to give a formula for the stopping power due not only to excitation and ionization of the stopping atoms, but also to the elastic Coulomb collisions of ion and nucleus of the stopping atom.

The contribution of the former to the stopping power (i.e., the excitation and ionization of atoms in the stopping medium) is the only effect included by Bohr, Bethe, and Bloch in their three theories discussed above. For specific energies above 1.0 MeV/amu, we may neglect all other contributions to the slowing down of the ion because this electronic stopping power is usually more than two orders of magnitude greater than any other contribution. However, as discussed by Bohr (1948), in that region of ( $\varepsilon$, $Z_1$, $Z_2$) space defined by small $\varepsilon$ and especially for large $Z_1$ and large $Z_2$, the slowing down of the ion due to elastic Coulomb collisions between the ion and nuclei of the stopping medium (i.e., nuclear Coulomb stopping power) affords the major contribution to the stopping power.

LSS have found it convenient to express their theory in dimensionless units. Their unit corresponding to distance is

$$\zeta = 4 \pi a^2 N_a \left[ \frac{A_1}{(A_1 + A_2)^2} \right] R , \qquad (7)$$

where $N_a$ is Avogadro's number and

$$a = 0.8853\, a_0 \,(Z_1^{2/3} + Z_2^{2/3})^{-1/2} \tag{8}$$

where $a_0$ is $0.529 \times 10^{-8}$ cm, the first Bohr radius for hydrogen. The unit corresponding to energy is

$$\epsilon = 1.602 \times 10^{-6} \frac{a}{e^2} \left( \frac{A_1 \quad A_2}{A_1 + A_2} \right) \frac{\varepsilon}{Z_1 \, Z_2} \tag{9}$$

where a is given by eq. (8) and e is $4.803 \times 10^{-10}$, the electronic charge in esu. Now the LSS expression for the electronic stopping power is

$$\left( \frac{d\epsilon}{d\zeta} \right)_e = k\varepsilon^{\;1/2}, \tag{10}$$

where k is a constant given by

$$k = \xi \; 0.0793 \frac{Z_1^{1/2} \, Z_2^{\;1/2}}{(Z_1^{2/3} + Z_2^{2/3})^{3/4}} \; \frac{(A_1 + A_2)^{3/2}}{A_1^{\;3/2} \, A_2^{1/2}}, \tag{11}$$

where $\xi$ is of the order of $Z_1^{1/6}$. The volume of ( $\varepsilon$, $Z_1$, $Z_2$) space for which eq. (10) is valid is given by

$$Z_1 \text{ and } Z_2 \gg 1 \text{ and} \tag{12}$$

$$Z_1^{\;1/3} \geqslant 137\beta. \tag{13}$$

(LSS suggest $Z_1^{2/3} \geqslant 137\,\beta$ instead of inequality (13), but we find this to be an inadequate restriction).

The stopping power due to nuclear Coulomb collisions is not expressed in closed form by LSS because the Thomas-Fermi scattering cross section cannot be expressed in closed form. It is graphically

presented in fig. 2 in the dimensionless units of eqs. (7) and (9). The validity of this formulation is restricted by inequality (12). The contribution of this elastic component of the total stopping power is significant only in the region identified by inequality (13).

In fig. 3 we illustrate the volume of ( $\varepsilon$, $Z_1$, $Z_2$) space in which each of the above four theories is valid. The boundaries separating each of the regions are somewhat arbitrarily placed. The LSS theory is valid over a plane across most of the back of the box. (It is actually a slab of thickness given by $0.01 \lesssim \varepsilon \lesssim 0.5$ MeV/amu.) Bethe's theory with shell corrections is valid throughout perhaps a third of the box. It is valid over essentially all of the box for which r is unity. There is a small region in which Bloch's or Bohr's theory is valid and Bethe's theory is not valid. However, in this region r is less than unity, and uncertain. Thus the advantage of Bloch's or Bohr's theory over Bethe's in any region of the box is questionable. It is clear, at any rate, that over a large portion of the box there is no valid theory (see fig. 3) and no experimental data (see fig. 1).

We refer the reader to the literature for other surveys of stopping-power theory. For a development from first principles of the form of Bethe's theory used today, See Fano (1963). For a brief overview of the development of Bohr's and Bethe's theories see Turner (1967). For more comprehensive reviews of the same nature as presented here, see Bethe and Ashkin (1953) and Northcliffe (1963). For a general theoretical treatise on the interactions between heavy energetic charged particles and matter, including charge exchange and the relationship between the

classical and quantum mechanical approaches, See Bohr (1948). For a tabulation using Bethe's theory of stopping power and range of protons and mesons, see Barkas and Berger (1964). A recent and useful tabulation of ranges and stopping power of a variety of solid and gaseous stopping materials for heavy ions ($^{1}H$ through $^{257}Lw$) over the energy range $0.0125 \leq \varepsilon \leq 12$ MeV/amu is provided by Northcliffe and Schilling (1970). For an up-to-date discussion of several topics on the penetration of charged particles in matter, see NAS-NRC publication 1133 (1964). Of interest to the radiochemist and radiobiologist is a classical development of the relative energy deposition within the high-LET track core and the lower LET peripheral region of the heavy-ion track provided by Mosumder, Chatterjee, and Magee (1968).

## 1.2 Our Composite Method

The unique aspect of the research reported here is that nowhere else have stopping power and range been generated for such a large continuous volume of ($\varepsilon$, $Z_1$, $Z_2$) space where active charge exchange between ion and stopping medium occur. We have generated stopping power and ranges for all ions from hydrogen through uranium in any nongaseous stopping medium over the velocity interval from 0.01 to 1 000 MeV/amu continuously. Over this velocity interval the charge on the ion varies from less than 10% to 100% of its nuclear charge. The dE/dR maximum is contained in this interval for all ions. The generation of accurate stopping power for the very heavy ions in the region of dE/dR maximum is at this time a difficult undertaking. The techniques developed here are a first-order attempt to supply these data.

We expect and solicit critical appraisal.

There have been several efforts to produce stopping power tables for use by researchers, but these tables usually do not give values that are valid for that difficult and large region of ( $\varepsilon$, $Z_1$, $Z_2$) space in which active charge exchange occurs (see e.g., Barkas and Berger 1964, Janni 1966, Serre 1967, Trower 1966, and Williamson, Boujot, and Picard 1966). However, the recent tables by Northcliffe and Schilling (1970) do cover some of this region of active charge exchange.

The availability of experimental stopping power and the validity of the various theories are each restricted to its own region of ( $\varepsilon$, $Z_1$, $Z_2$) space as discussed above. Thus in developing our method for generating stopping power, it is convenient for us to divide ( $\varepsilon$, $Z_1$, $Z_2$) space into corresponding regions. We develop for each region its own technique and strive for continuity in stopping power at the boundaries. The division of ( $\varepsilon$, $Z_1$, $Z_2$) space is roughly illustrated in fig. 4. The depths of the low- and medium-low-specific-energy regions have been exaggerated in order to make them visible. The depth of the region for which $Z_1 \leq 10$ and $\varepsilon < 10$ has also been exaggerated.

## 2. METHOD

### 2.1 Method for $Z_1$ Less than Eleven

#### 2.1.1 Specific energy less than 10 MeV/amu

In this region of ( $\varepsilon$, $Z_1$, $Z_2$) space some experimental data are available. Active charge exchange occurs, making theoretical treatment

difficult. Thus we make maximum use of the experimental data. To do this we have modified a method proposed by Northcliffe (1963) for generating smooth stopping-power curves through experimental points. For further details see Steward (1968).*

2.1.2 Specific energy greater than 10 MeV/amu

In this region of ($\varepsilon$, $Z_1$, $Z_2$) space ($Z_1 \leq 10$, $\varepsilon \geq 10$ MeV/amu), the ions are completely stripped of orbital electrons, so that we may extend to all ions the proton stopping power by means of the formula $dE/dR = Z_1^2 (dE/dR)_p$, where $dE/dR$ is the stopping power of the ion of charge $Z_1$ at the same velocity and in the same stopping material as for the proton whose stopping power is $(dE/dR)_p$. This transformation is consistent with Bethe's theory. The proton stopping power is obtained from Barkas and Berger's (1964) polynomial fit to Bethe's theory.

2.1.3 Ion mean ranges for $Z_1 \leq 10$

The mean range of these ions in units of g/cm$^2$ is obtained from the expression

$$R(\varepsilon) = 2\left(\frac{0.01\, A_1}{S(\varepsilon = 0.01)}\right) + A_1 \int_{0.01}^{\varepsilon} \frac{d\varepsilon'}{S(\varepsilon')}$$

where $S(\varepsilon)$ is the stopping power of the ion at specific energy $\varepsilon$ calculated as indicated above. The first term of this expression is an estimate of the range of a 0.01-MeV/amu ion. This assumes that the stopping power is proportional to $\varepsilon^{1/2}$ below 0.01 MeV/amu.

*This document is available from the authors upon request.

## 2.2. Method for $Z_1$ Greater than 10

### 2.2.1 Low-specific-energy region ($137\,\beta \leq Z_1^{1/3}$)

In this region the ions are rapidly capturing electrons, thus losing effective charge. The stopping power or linear energy transfer (LET) is decreasing with decreasing velocity. The LET of the ions is not large compared with that in the other regions. This is the region of the recoil nucleus or nuclear reaction products. Charged particles in this region are of particular concern to the radiobiologist because the radiation dmage may be qualitatively different from the damage for higher-energy particles (see, e.g., Kistemaker, Detteer, Saunders, and Snook 1967 and Jung 1967).

LSS have developed a theory for this velocity region (see section 1.1). Their theory for the electronic stopping power is given by eq. (10). By modifying the constant k (eq. 11) very slightly we obtained better agreement with experimental fission-product range data in Al and U and stopping-power data for Ne and Ar ions in Al. We increased the constant by 1.5% and changed $\xi$ from $Z_1^{1/6}$ to $Z_1^{0.207}$. Making these modifications, along with a change of units, we obtain for the electronic stopping power

$$\left(\frac{dE}{dR}\right)_e = C_e \quad \varepsilon^{1/2}, \qquad (14)$$

where $C_e = 7.39\times 10^4\,(Z_1^{1.207}\,Z_2)/[A_2\,(Z_1^{2/3} + Z_2^{2/3})^{3/2}]$. The theory developed by LSS for the nuclear Coulomb stopping power is represented by the curve in fig. 2. By fitting a function to this curve and changing units again, we get

$$\left(\frac{dE}{dR}\right)_n = C_n \; \varepsilon^{1/2} \exp\left[-45.2(C_n' \; \varepsilon)^{0.277}\right]. \tag{15}$$

where

$$C_n = 4.14 \times 10^6 \left(\frac{A_1}{A_1 + A_2}\right)^{3/2} \left(\frac{Z_1 \; Z_2}{A_2}\right)^{1/2} \left(Z_1^{2/3} + Z_2^{2/3}\right)^{-3/4}.$$

and

$$C_n' = \frac{A_1 \; A_2}{Z_1 \; Z_2} \; \frac{1}{A_1 + A_2} \; \left(Z_1^{2/3} + Z_2^{2/3}\right)^{-1/2}.$$

Thus, for the low-specific-energy region, the total stopping power is given by

$$\left(\frac{dE}{dR}\right) = \left(\frac{dE}{dR}\right)_e + \left(\frac{dE}{dR}\right)_n \tag{16}$$

where $(dE/dR)_e$ and $(dE/dR)_n$ are given in eqs. (14) and (15) respectively.

### 2.2.2. Medium-low-specific-energy region ($Z_1^{1/3} < 137\,\beta \leq 9$)

This is a narrow region connecting the variable upper boundary of the low-specific-energy region with the fixed lower boundary of the medium-high-specific-energy region. No experimental data nor theories available for this region are satisfactory for estimating the stopping power. However, since this region is so narrow, a cubic polynomial, matching slope and magnitude of the stopping power at both boundaries provides the stopping-power relation within the

### 2.2.3 Medium-high-specific-energy region ($9 < 137\,\beta \leq 3\,Z_1$)

This region is bounded on the high side by the velocity at which the ion can be considered to be completely stripped of electrons. It is bounded on the low side by velocities for which we believe the method described below cannot adequately provide stopping power.

Our method uses charge-state data derived from range-energy data available for Ar ions incident upon Al. These charge-state data are generalized to all ions for which $Z_1 > 10$ and all stopping media as described in detail by Steward (1968). A plot of this charge state appears in fig. 5. The stopping power in this medium-high-specific-energy region now becomes

$$(dE(\varepsilon)/dR = Z_1^2\, r^2\, (dE/(\varepsilon)/dR)_p,$$

where the proton stopping power $(dE/dR)_p$ is given by the polynomials of Barkas and Berger (1964).

### 2.2.4. High-specific-energy region ($137\,\beta > 3\,Z_1$)

In this region the ion is assumed to be completely stripped of its orbital electrons and the conditions for the validity of the Born approximation are met. Thus Bethe's theory gives the stopping power

$$dE(\varepsilon)/dR = Z_1^2\, (dE(\varepsilon)/dR)_p,$$

where $(dE/dR)_p$ is given by the Barkas and Berger polynomial as before.

### 2.2.5. Ion mean range for $Z_1 > 10$

The mean range of ions is given by the integral of the reciprocal of the stopping powers calculated above.

## 2.3 Compounds and Mixtures

When there is more than one atomic component to the stopping medium, as in mixtures and compounds, we assume that the stopping power of each component acts independently and is thus additive to the others. This is Bragg's rule, which can be expressed

$$\frac{dE}{dR} = \frac{1}{\rho} \sum_i \rho_i \left(\frac{dE}{dR}\right)_i ,$$

where $(dE/dR)_i$ is the stopping power of the ith component in density-independent units such as MeV/(g/cm$^2$), $\rho_i$ and $\rho$ are the partial density of the ith component and the overall density of the medium respectively ($\rho = \sum_i \rho_i$). The validity of Bragg's rule is discussed in section 3.7.

# 3. DISCUSSION OF METHOD

## 3.1 Experimental Data

In the region of ($\varepsilon$, $Z_1$, $Z_2$) space defined by $\varepsilon \leq 10$ and $Z_1 \leq 10$, our method is designed to closely follow smooth curves placed through available experimental stopping-power data. Northcliffe (1963) has summarized the availability of these data and he has plotted them for H, He, B, C, N, O, F, and Ne ions each incident upon C, Al, Ni, Ag, and Au. The uncertainty for the data points quoted by the investigators commonly varies from ± 3% to ± 15%.

We are reluctant to estimate error limits for the smooth curves which Northcliffe places through these data, but we have more confidence in them than we do in many of the raw experimental points. We expect

the error limits are greatest for $\varepsilon < 0.1$ MeV/amu, smaller for $0.1 < \varepsilon < 10$ MeV/amu. Also we expect the error limit to increase with increasing $Z_1$.

### 3.2. Gaseous vs Nongaseous Stopping Media

Stopping power and ranges calculated by our method may not be valid for gaseous stopping media. Lassen (1951) discovered that the most probable charge state of partially stripped ions differed in gaseous and nongaseous stopping material. From his data it appears that fission products in solids have a stopping power greater by more than a factor of two than in rarefied gases. Bohr and Lindhard (1954) suggested that this difference was the result of the fact that in solids an electronic level of the ion excited by one collision has a shorter time interval in which to relax before the next collision occurs, therefore this electron is more apt to be in an excited level, and thus more readily removed, at the time of the subsequent collision in solids than in gases. Grodzins, Kalish, Murnick, Van de Graaff, Chmara, and Rose (1967) found the root-mean-square charge of iodine ions of $\varepsilon = 1.2$ to be about 30% greater when stripped by carbon foils than when stripped by argon gas. Ryding, Wittkower, and Rose (1969) determined that iodine ions of $\varepsilon = 0.035$ have 17% greater mean charge in the denser of two rarefied gases. All these data are compatible with Lassen's original findings and Bohr and Lindhard's physical interpretation.

Pierce and Blann (1968) distinguish between the root-mean-square charge and the effective charge of the ion. The effective charge is defined

as the value which, when substituted for $rZ_1$ in Bethe's theory (eqs. 5 and 6) gives the correct stopping power. They find that the rms charge of ions emerging from solid foils is indeed greater than that of ions emerging from gases. However, the effective charge of the ions in these two cases are the same. Pierce and Blann suggest that ions may indeed have identical charges while traversing solid and gaseous stopping media, but the ion is then robbed of some of its electrons at the surface of a solid as the ion leaves. They suggest an interesting physical explanation for this phenomenon. Martin and Northcliffe (1962) also found the effective ion charge to be the same in aluminum and most gases.

Even if the excess in ion charge found after emerging from solids over that found after emerging from gases is indeed the result of some surface phenomenon, as suggested by Pierce and Blann, it nevertheless appears from the findings of Ryding et al. that a density effect of the type described by Bohr and Lindhard may still exist.

The question of the degree to which the ion charge is influenced by the density of the stopping medium whenever the ion is not completely ionized appears to be not entirely resolved. Since some effect does exist, we suggest that the stopping powers calculated here be used with caution whenever the stopping medium is a gas and the ion is not completely stripped of electrons. For $Z_1 \leq 10$ and $\varepsilon \leq 10$ MeV/amu, experimental stopping powers in $H_2$ gas are built into our calculational technique. From the discussion above and from the data of Martin and Northcliffe (1962), it is not clear in what direction this may cause the calculation to err. If this introduces any error at all, it will occur only

whenever the ion is not completely stripped, the ion has $Z \leq 10$, and the stopping medium is hydrogenous (i.e., water, tissue, a hydrocarbon, etc.).

### 3.3. Bethe's Theory

Barkas and Berger (1964) have determined that their polynomial, which we use instead of Bethe's theory, has a root-mean-square percentage deviation from 600 points calculated by Bethe's Theory of 0.6% for the ion range and 1.3% for its stopping power. The maximum error for the range is 2.8%. Therefore the overall accuracy of our method where Bethe's Theory is valid (see fig. 3d) should be between 1% and 3%.

### 3.4. LSS Theory

In developing their theories which are based upon the Thomas-Fermi model of the atom, 1961, 1963 (referred to as LSS), Scharff, and Schiott treat separately the effect of elastic collisions between the ion and the Coulomb field of the nuclei in the stopping material, and the effect of inelastic collisions between the ion and the atomic electrons in the stopping material. The assumption that these two effects are uncorrelated may result in systematic overestimation of the stopping power, according to LSS. LSS also warn that the validity of this theory is uncertain for $\varepsilon < 10^{-2}$ MeV/amu, since the Thomas-Fermi treatment of the atom is a crude approximation when the ion and atom do not come close to each other. Others have been critical of these theories too, particularly of the theory for the stopping due to inelastic collisions (see eqs. 10 and 11). The variation of k (eq. 11) with $Z_1$ and $Z_2$ has

been found to be imperfect, and the variation of stopping power with velocity has been found to differ somewhat from $\varepsilon^{1/2}$ (eq. 10). (For a more detailed discussion of these criticisms see Steward 1968.)

However, wherever we have available direct comparison with experimental data, the ranges calculated in the low-specific-energy region by means of eq. (16), which is an only slightly modified LSS theory, are usually very close to the experimental values. We calculate ranges which are usually within 5% to 10% of the ranges measured for Dy ions in Al by Gilat and Alexander (1964) (see fig. 8 of Steward 1968). Also we have collected $^{235}U$ fission-product ranges from several reported experiments which are summarized in Hyde (1964), and we obtain good agreement with ranges calculated by our techniques, as demonstrated in Tables 1 and 2.

Since the experimental ranges are a measure of the distance the ion travels projected onto the initial direction of flight, we should compare the experimental ranges with a calculation of the mean projected range. The path-length range, obtained by our method, is the total mean distance the ion travels no matter how twisted its path may be. The difference between the projected and path-length ranges is due to multiple scattering of the ion by nuclei in the stopping material. As one would expect, this difference is the more significant the lighter the ion and the heavier the nuclei of the stopping medium. In order to calculate the projected range for these experimental comparisons, two computer programs were written. One calculates the mean projected range of the ions and the other calculates the difference between the mean projected

range and the mean path-length range. It is these programs that have provided the projected ranges included in Tables 1 and 2. The computer programs and the method used in each are discussed by Steward (1968).

### 3.5. Medium-Low-Specific-Energy Region

We calculate ranges that are within 5% to 10% of the ranges measured for Cl ions in Al by Kaplan and Ewart (1966) (see fig. 9 of Steward 1968). Since we believe the velocities of these Cl ions are above the region of validity for the LSS theory, and are thus in our medium-low-specific-energy region, this agreement is more a confirmation of the technique we use to calculate ranges in this higher-energy region than it is a confirmation of LSS theory. That the ranges of these Cl ions were measured at such high velocities ($0.2 \leq \varepsilon \leq 0.9$ MeV/amu) may have contributed to the finding by Kaplan and Ewart that the variation of stopping power with energy was less pronounced than $\varepsilon^{1/2}$.

### 3.6. Medium-High-Specific-Energy Region

There are two major assumptions implicit in our calculational technique used in the medium-high-specific-energy region which prevent our generating stopping power in this region with theoretical rigor. One assumption is that Bethe's theory is valid in this region of ($\varepsilon$, $Z_1$, $Z_2$) space. This is not true, since neither inequality (3) nor (4), one of which is required for use of the Born approximation, is always fulfilled. Inequality (3) is nowhere well satisfied, since the high-velocity boundary of this region is $3 Z_1 = 137 \beta$. Therefore we cannot be certain that Bethe's theory will generate correct stopping power unless inequality (4)

is satisfied, that is to say unless the nuclei of the stopping medium are heavier than the ion. It is clear then that we cannot use Bethe's theory here with rigor whenever the stopping material is water, tissue, or any hydrocarbon. However, for reasons discussed by Steward (1968), we believe this method to be fairly good, and at least the best available. The second assumption is that r (see fig. 5), which is a function only of $X = 137\ \beta/Z_1^{g}$, can successfully give the charge state of all ions in all stopping media throughout the medium-high-specific-energy region. Arguments favoring the assumption are presented by Steward (1968).

### 3.7. Bragg's Rule

We use Bragg's rule in order to calculate the stopping power of compounds and mixture throughout ($\varepsilon$, $Z_1$, $Z_2$) space. In the low-velocity portion of this space, e.g., $\varepsilon < 1$ MeV/amu, Bragg's rule is less valid than for the higher-velocity regions. The main reason for this is that as the velocity of the ion decreases, the more tightly bound inner electronic shells of the stopping medium play a smaller role in the stopping process. Thus the most loosely bound shells, for example the valence shell, contribute a larger fraction of the stopping. Since it is primarily the valence shell whose energy levels are modified by molecular binding, it is primarily the low-velocity ions whose stopping rate will be affected by the chemical state of the atomic components of the stopping medium. As a corollary to this line of reasoning, we wish to point out that for all ion velocities one expects that compounds of the lighter atoms, such as H, C, N, and O, will not follow Bragg's rule so well as compounds of heavier atoms. This is because larger fractions of the total electron

clouds of the lighter atoms are valence electrons. Thus, for $\varepsilon \ll 1$ MeV/amu, our calculation of stopping power in compounds may suffer from the use of Bragg's rule, particularly when the stopping medium is tissue, a hydrocarbon, water, or other hydrogenous compound.

The error introduced by using Bragg's rule is not large in most cases. Thompson (1952) has found that the use of Bragg's rule for calculating the stopping power of hydrocarbons for high-energy protons (200 to 340 MeV) introduces an error of the order of 1 to 2% or less. Aniansson (1961) makes similar findings for 5.3-MeV $\alpha$ particles. Reynolds, Dunbar, Wenzel, and Whaling (1953) have found that Bragg's rule introduces an error in the calculation of stopping power of gaseous H, C, N, and O compounds which increases to more than 2% as the proton energy decreases below 0.15 MeV.

## 4. RESULTS

The computer program that incorporates our method has generated a sampling of ranges and stopping powers to be displayed here. The ions chosen are H, $^{4}$He, $^{12}$C, $^{20}$Ne, $^{40}$Ar, $^{84}$Kr, $^{131}$Xe, and $^{222}$Rn. Data are presented for each of these ions incident upon water, aluminum, copper, silver, lead, and uranium.

In figs. 6 through 11 stopping power is plotted as a function of specific energy. One of the conspicuous features of these curves is the difference in behavior in the low-specific-energy region between the ions for $Z_1 > 10$ and for $Z_1 \leq 10$. This reflects the fact that a completely different method is used to calculate the stopping power in these two cases. For $Z_1 > 10$, eq. (16) is used. The increasing contributions

of the nuclear Coulomb stopping-power term as $Z_1$ increases and $\varepsilon$ decreases cause the slope of the curves to decrease under these conditions. According to LSS, the assumption that the nuclear and electronic stopping powers are separable may lead to a systematic overestimation of the stopping power in this low-specific-energy region. The smoothed experimental stopping power which we try to duplicate with our method for $Z_1 \leqslant 10$ does not usually show a decreasing slope for decreasing velocity because the scatter of the experimental points is usually too great to permit the resolution of such fine detail. Thus the decreasing slope for decreasing velocity may be overestimated for Ar ions and underestimated for Ne ions, leading to a discontinuity in the systematic change of behavior across the $Z_1 = 10$ boundary.

It may be useful to examine this discontinuity in more detail in order to obtain a measure of the accuracy of our method for $Z_1 \approx 10$. In fig. 12 the lower pair of curves are plots of the stopping power of Ne ions in Al by both methods. The agreement between these two curves is very good. The difference between their magnitudes is ± 10%. The upper pair of curves in fig. 12 compares the two methods for Ne ions in water. The agreement is not so good here. There are two main reasons for this, and both have to do with the difficulty of treating hydrogenous stopping media. First, the experimental stopping power of hydrogen used by the method for $Z_1 \leqslant 10$ is the stopping power of gaseous hydrogen. The ions at low velocities therefore may have a lower charge than they would in condensed hydrogen, as discussed in section 3.2. Second, the Thomas-Fermi atomic model, which is used in the low-specific-energy region for $Z_1 > 10$, cannot be applied with

rigor to hydrogenous stopping media, since the statistical model cannot properly be applied to hydrogen. The method for $Z_1 > 10$ is more properly applied to stopping media heavier than hydrogen.

In figs. 13 through 18 the stopping power is plotted as a function of ion residual path-length range. Points of constant specific energy are indicated by symbols at 0.01, 0.1, and 1.0 MeV/amu and by curves at 5, 10, 50, 100, 200, 300, and 500 MeV/amu. From fig. 13, for instance, we see that a 5-MeV/amu $^{20}Ne$ in water has an LET of 7500 MeV/(g/cm$^2$) and a range of 100 microns. The discontinuity in behavior across the $Z_1 = 10$ boundary discussed above is apparent here also.

The H-He, C-Ne, and Xe-Rn crossovers of fig. 13 are not so bizarre as they probably appear, because velocity and not residual range is the natural variable of stopping power. Let us discuss these crossovers one at a time. Since He has four times the mass but only twice the charge of H, the two ions have the same range for constant velocity when $r = 1$ because range is proportional to $A_1/(r Z_1)^2$. This makes it easier for the He and H curves to cross over at some low velocity where $r \approx 1$ for H ions but $r < 1$ for He ions.

The error we introduced into fig. 13 at low velocity for $Z_1 \leq 10$ by using the experimental stopping power in gaseous hydrogen instead of condensed hydrogen may have the effect of introducing a value of r that is too small. Since stopping power is proportional to $(r Z_1)^2$, the error has the effect of moving a curve plotted on the coordinates of fig. 13 down and to the right of where it should be. Neon ions would be affected by this error at higher velocities than carbon ions, so the magnitude of the C-Ne crossover may be accentuated by this error.

All three of these crossovers occur in regions where we have relatively low confidence in our method. Thus they may not exist in reality and may be an artifact of the method. This is certainly the case for the Xe-Rn crossovers of fig. 13. These two curves cross over only slightly in the medium-low-specific-energy region. It is in this region that we extend the stopping power from the boundaries into the region by means of a cubic polynomial determined by the slope and magnitude of the stopping power at the boundaries. In fig. 13, where two curves approach each other near this medium-low-specific-energy region, the curvature provided by the cubic can easily be sufficiently erroneous to allow crossovers such as this Xe-Rn crossover.

In figs. 19 through 24 the velocity is plotted as a function of residual range. The discontinuity in the systematic change of behavior across the $Z_1 = 10$ boundary, as discussed above, is apparent in these curves below 0.1 MeV/amu.

## SUMMARY

A method is discussed for calculating range and stopping-power data for any heavy ion with $0.01 \leq \varepsilon \leq 1000$ MeV/amu incident upon any nongaseous stopping medium. The method is incorporated into a FORTRAN IV computer program. Results are presented for H, $^{4}$He, $^{12}$C, $^{20}$Ne, $^{40}$Ar, $^{84}$Kr, $^{131}$Xe, and $^{222}$Rn ions each incident upon $H_2O$, Al, Cu, Ag, Pb, and U.

For ions at low energy with $Z \leq 10$, the program uses experimental data. For ions with $Z > 10$, the nuclear and electronic stopping-

power theory developed by Lindhard et al. is adjusted to fission-product range data at low energy; for intermediate energies, charge-state data developed from experimental Ar range-energy data in Al are extended to other ions and stopping media. Bethe's theory is used for all ions at high energy. The particle ranges calculated by the method are path-length ranges and do not include the effects of multiple scattering.

## ACKNOWLEDGMENTS

This research was supported by the Atomic Energy Commission, in part through its Special Fellowship Program in Health Physics, which is administered by the Oak Ridge Associated Universities, and in part through its support of the Biomedical Division of the Lawrence Radiation Laboratory at Berkeley, California.

We are indebted to Mr. Wade Patterson and the entire Health Physics Department of the Lawrence Radiation Laboratory at Berkeley for their cooperation and support.

We acknowledge the valuable support of Professor Cornelius A. Tobias.

Table 1. Ranges in Al calculated by the program compared with the experimental fission-product ranges (Hyde 1964).

| Ion | Estimated specific energy (MeV/amu) | Range ($mg/cm^2$) | | |
|---|---|---|---|---|
| | | | Calculated | |
| | | Experimental | Projected | Path length |
| $^{89}_{38}Sr$ | 1.12 | 4.09 | 4.12 | 4.15 |
| $^{115}_{48}Cd$ | 0.613 | 3.32 | 3.14 | 3.18 |
| $^{140}_{56}Ba$ | 0.489 | 2.98 | 3.03 | 3.07 |
| $^{144}_{58}Ce$ | 0.437 | 2.76 | 2.84 | 2.87 |

Table 2. Experimental fission-product ranges in U compared with ranges calculated by the program (Hyde 1964).

| Ion | Estimated specific energy (MeV/amu) | Range (mg/cm$^2$) | | |
|---|---|---|---|---|
| | | | Calculated | |
| | | Experimental | Projected | Path length |
| $^{89}_{38}Sr$ | 1.12 | 11.55 | 11.76 | 12.82 |
| $^{109}_{46}Pd$ | 0.816 | 10.14 | 9.91 | 10.87 |
| $^{115}_{48}Cd$ | 0.613 | 9.52 | 8.35 | 9.27 |
| $^{140}_{56}Ba$ | 0.489 | 8.74 | 7.64 | 8.48 |
| $^{144}_{58}Ce$ | 0.437 | 8.37 | 7.04 | 7.85 |

## APPENDIX: NOTATION

| Symbol | Description of Symbol in Order of Appearance |
|---|---|
| $\varepsilon$ | The specific energy of the ion units of MeV per atomic mass unit of the ion |
| $\beta$ | The ratio of the velocity of the ion to that of light in a vacuum |
| E | Kinetic energy of the ion in units of MeV |
| $A_1$ | Atomic weight of the ion |
| V | The velocity of the ion (cm/sec) |
| $Z_1$ | The atomic number of the ion (projectile) |
| $Z_2$ | The atomic number of the stopping medium (target) |
| r | The ratio of the root-mean-square actual charge of the ion $Z_{1_{eff}}$ to that of its nucleus $Z_1$ |
| $\hbar$ | Plank's constant divided by $2\pi$ |
| m | The mass of the ion |
| $\frac{dE}{dR}$ | Stopping power in units of MeV/(g/cm$^2$). |
| B | The stopping number (dimensionless) |
| $A_2$ | Atomic weight of the stopping medium |
| ln | Natural logarithm |
| $m_e$ | The rest mass of an electron (gm) |

| Symbol | Description of Symbol in Order of Appearance |
|---|---|
| $e$ | The charge of an electron = $4.803 \times 10^{-10}$ (esu). |
| $c$ | The velocity of light |
| $I$ | Average atomic excitation potential of the stopping medium |
| $C_i$ | Shell corrections for the ith shell |
| $\delta$ | Polarization correction for the stopping medium |
| $\psi(x)$ | $\frac{d \ln \Gamma(x)}{dx} = \frac{1}{\Gamma(x)} \frac{d\Gamma(x)}{dx}$ = logarithmic derivative of the gamma function |
| Re | Real part of a complex number |
| $\zeta$ | The dimensionless unit corresponding to range are to Lindhard et al. |
| $N_a$ | Avogadro's number |
| $R$ | Ion range (g/cm$^2$) |
| $a_0$ | The radius of the first Bohr orbit in hydrogen = $0.529 \times 10^{-8}$(cm) |
| $\epsilon$ | The dimensionless unit corresponding to energy due to Lindhard et al. |
| $k$ | Electronic stopping-power constant from Lindhard et al. see Eq. (11) and LSS (1963). |
| $\xi$ | A number near 1 and of the order of $Z_1^{1/6}$ |
| $\left(\frac{dE}{dR}\right)_p$ | Stopping power MeV/(g/cm$^2$) for protons |
| $S$ | Identical to eD/dR above. This symbol is used where a less cumbersome notation is desirable. |

| Symbol | Description of Symbol in Order of Appearance |
|---|---|
| $\left(\frac{dE}{dR}\right)_e$ | Electronic stopping power MeV/(g/cm$^2$) |
| $\left(\frac{dE}{dR}\right)_n$ | Nuclear Coulomb stopping power MeV/(g/cm$^2$) |
| $Z_{1_{eff}}$ | $r\,Z_1$, the root-mean-square charge of the ion |
| $\rho$ | Density of the stopping medium |

## REFERENCES

Aniansson, Gunnar, 1961, Trans. Roy. Inst. Tech Stockholm 178, 1.

Aras, N. K., Menon, M. P., and Gordon, G. E., 1965, Nucl. Phys. 69, 337.

Barkas, Walter H., and Berger, Martin, J., 1964, in Studies in Penetration of Charged Particles in Matter (Washington, D.C., National Academy of Sciences–National Research Council Publication 1133), p. 103.

Bethe, H. A., 1930, Ann. Physik 5, 325. (In German.)

Bethe, H. A., 1932, Z. Physik 76, 293. (In German.)

Bethe, H. A., and Ashkin, J., 1953, "Experimental Nuclear Physics," edited by E. Segrè, Vol. 1 (New York, John Wiley and Sons, Inc.) p. 166.

Bichsel, H., 1961, University of Southern California Report No. 3 [Contract AT (04-3)-1367].

Bloch, F., 1933, Ann. Physik 16, 285. (In German.)

Bohr, N., 1913, Phil. Mag. 25, 10.

Bohr, N., 1915, Phil. Mag. 30, 581.

Bohr, N., 1948, Kgl. Danske Videnskab. Selskab Mat.-Fys. Medd. 18, 8.

Bohr, Niels, and Lindhard, Jens, 1954, Kgl. Danske Videnskab. Selskab Mat.-Fys. Medd. 28, 7.

Fano, U. 1963, Ann. Rev. Nucl. Sci. 13, 1 (also reprinted as Appendix A in NAS-NRC, 1964).

Gilat, Jacob, and Alexander, John M., 1964, Phys. Rev. 136, B1298.

Grodzins, L., Kalish, R., Murnick, D., Van de Graaff, R. J., Chmara, F., and Rose, P. H., 1967 Phys. Letters 24B, 282.

Hyde, Earl K., 1964, "The Nuclear Properties of the Heavy Elements," Vol. III "Fission Phenomena" (Englewood Cliffs, New Jersey, Prentice-Hall, Inc., New Jersey).

Janni, Joseph F., 1966, Air Force Weapons Laboratory Report AFWL-TR-65-150.

Jung, H., 1967, "Radiation Research, Proceedings of the Third International Congress of Radiation Research held at Cortina d'Ampezzo, Italy, June-July, 1966" (Amsterdam, North Holland Publ. Co.; New York, John Wiley and Sons, Inc.) p. 410.

Kaplan, Morton, and Ewart, Alan, 1966, Phys. Rev. 148, 1123.

Kistemaker, J., Detteer, F. J., Sanders, J., and Snook, G., 1967, "Radiation Research, Proceedings of the Third International Congress of Radiation Research held at Cortina d'Ampezzo, Italy, June-July, 1966" (Amsterdam, North Holland Publ. Co.; New York, John Wiley and Sons, Inc.), p. 68.

Lassen, N. O., 1951, Kgl. Danske Videnskab. Selskab Mat.-Fys. Medd. 26, 5.

Lindhard, J., and Scharff, M., 1961, Phys. Rev. 124, 128.

Lindhard, J., Scharff, M., and Schiott, H. E., 1963, Kgl. Danske Videnskab. Selskab Mat.-Fys. Medd. 33, 14.

Litton, Gerald M., 1967, Lawrence Radiation Laboratory Report UCRL-17391, Feb.

Litton, G. M., Lyman, J., and Tobias, C. A., 1968, Lawrence Radiation Laboratory Report UCRL-17392-Rev., May.

Livingston, M. S., and Bethe, H. A., 1937, Rev. Mod. Phys. 9, 261.

Martin, F. W., and Northcliffe, L. E., 1962, Phys. Rev. 128, 1166.

Mott, N. F., 1931, Proc. Cambridge Phil. Soc. 27, 533; also see Mott, N. F., and Massey, H. S. W., "The Theory of Atomic Collisions" (Oxford, Clarendon Press, 1965), p. 615.

Mozumder, A., Chatterjee, A., and Magee, J. L., 1968, Theory of Radiation Chemistry, IX. Model and Structure of Heavy Particle Tracks in Water. Advan. Chem. Ser. 81, 27.

NAS-NRC, 1964, "Studies in Penetration of Charged Particles in Matter" (Washington, D.C., National Academy of Sciences—National Research Council Publication 1133).

Northcliffe, L. C., 1963, Ann. Rev. Nucl. Sci. 13, 67, also reprinted as Appendix B in NAS-NRC (1964).

Northcliffe, L. C., Schilling, R. F., 1970, Nuclear Data 7, 233.

Pierce, T. E., and Blann, Marshall, 1968, Phys. Rev. 173, 390.

Reynolds, H. K., Dunbar, D. N. F., Wenzel, W. A., and Whaling, W., 1953, Phys. Rev. 92, 742.

Ryding, G., Wittkower, A., and Rose, P. H., 1969, Phys. Rev. 184, 93.

Serre, Claude, 1967, CERN-67-05. (In French.)

Steward, Palmer G., 1968 (Ph.D. Thesis), Lawrence Radiation Laboratory Report UCRL-18127, May.

Thompson, T. J., 1952, Ph.D. Thesis, University of California Radiation Laboratory Report UCRL-1910, Aug.

Trower, W. Peter, 1966, Lawrence Radiation Laboratory Report UCRL-11647 Rev., Sept.

Turner, J. E. 1967, Health Phys. 13, 1255.

Walske, M. C. 1952, Phys. Rev., 88, 1283.

Walske, M. C. 1956, Phys. Rev. 101, 940.

Whaling, Ward 1958, Encyclopedia of Physics Vol. 34 (Springer-Verlag, Berlin).

Williamson, C. F., Boujot, J. P., and Picard, J. 1966, CEA-R-3042.

## FIGURE CAPTIONS

Fig. 1. A geometric view of that part of ( $\varepsilon$ , $Z_1$, $Z_2$) space for which $0.01 \leq \varepsilon \leq 500$, $1 \leq Z_1 \leq 92$, and $1 \leq Z_2 \leq 92$. The regions of this subspace for which experimental stopping power is available are indicated by the slabs covering the bottom and part of the back of the box (accelerated particle data) and the two lines on the back of the box (fission product range data).

Fig. 2. The nuclear Coulomb stopping power for heavy ions at low velocities. The $\zeta$-$\epsilon$ units used in this figure (see text) allow one curve to provide this stopping power for any ion in any medium.

Fig. 3. In these four views of ( $\varepsilon$ , $Z_1$, $Z_2$) space we depict the regions of validity of four different theories. The theories are: (a) Lindhard et al. (1963); (b) Bohr (1913); (c) Bloch (1933); and (d) Bethe (1930).

Fig. 4. In this view of ( $\varepsilon$ , $Z_1$, $Z_2$) space we illustrate the regions into which we divide this space. In the high-specific-energy region (H) and the region for which $Z_1 < 10$ and $\varepsilon \geq 10$ we use Bethe's theory directly. In the medium-high-specific-energy region (MH) we use Bethe's theory with charge-state data. In the medium-low-specific-energy region (ML) we use a cubic polynomial (see text). In the low-specific-energy region (L) we use Lindhard's theories. In the region for which $Z_1 \leq 10$ and $\varepsilon < 10$ we use experimental data.

Fig. 5. Here r is the charge state $Z_{1_{eff}} / Z_1$, and $X = 137\,\beta/Z_1^g$ where g is given by

$$g = 2/3 \qquad \text{for } 137\,\beta \leq Z_1^{2/3},$$

$$g = \frac{137\,\beta + 4Z_1 - 3Z_1^{2/3}}{6\,Z_1 - 3\,Z_1^{2/3}} \qquad \text{for } Z_1^{2/3} < 137\,\beta < 2\,Z_1,$$

$$g = 1 \qquad \text{for } 2\,Z_1 \leq 137\,\beta \leq 3\,Z_1.$$

Fig. 6. Stopping-power curves as a function of specific energy for various ions in water as calculated by the computer program. At the top of the figure, values of $\beta = V/c$ are displayed. (The Ne and C curves touch at about 0.04 MeV/amu due to an inaccuracy in the program. Our method overestimates the experimental stopping power for carbon ions in hydrogen at 0.04 MeV/amu by 14% and underestimates it for Ne ions by 6%.)

Fig. 7. Stopping-power curves as a function of specific energy for various ions in aluminum as calculated by the computer program. At the top of the figure, values of $\beta = V/c$ are displayed.

Fig. 8. Stopping-power curves as a function of specific energy for various ions in copper as calculated by the computer program. At the top of the figure, values of $\beta = V/c$ are displayed.

Fig. 9. Stopping-power curves as a function of specific energy for various ions in silver as calculated by the computer program. At the top of the figure, values of $\beta = V/c$ are displayed.

Fig. 10. Stopping-power curves as a function of specific energy for various ions in lead as calculated by the computer program.

At the top of the figure, values of $\beta = V/c$ are displayed.

Fig. 11. Stopping-power curves as a function of specific energy for various ions in uranium as calculated by the computer program. At the top of the figure, values of $\beta = V/c$ are displayed.

Fig. 12. Stopping-power curves as a function of specific energy for a Ne ion in aluminum (lower pair) and in water (upper pair). The member of each pair of curves that shows a decreasing slope for decreasing velocity at very low velocity is calculated by the method normally used only for ions with $Z_1 > 10$. The other member of each pair of curves is calculated by the method used for $Z_1 \leq 10$.

Fig. 13. Stopping-power curves as a function of residual range for various ions in water as calculated by the computer program. Various ion specific energies in units of MeV/amu are designated on each curve by symbols for $\varepsilon \leq 1.0$ and by curves of constant velocity for $\varepsilon \geq 5$. The H-He, C-Ne, and Xe-Rn crossovers are discussed in the text.

Fig. 14. Stopping-power curves as a function of residual range for various ions in aluminum as calculated by the computer program. Various ion specific energies in units of MeV/amu are designated on each curve by symbols for $\varepsilon \leq 1.0$ and by curves of constant velocity for $\varepsilon \geq 5$.

Fig. 15. Stopping-power curves as a function of residual range for various ions in copper as calculated by the computer program. Various ion specific energies in units of MeV/amu are designated

on each curve by symbols for $\varepsilon \leqslant 1.0$ and by curves of contant velocity for $\varepsilon \geqslant 5$.

Fig. 16. Stopping-power curves as a function of residual range for various ions in silver as calculated by the computer program. Various ion specific energies in units of MeV/amu are designated on each curve by symbols for $\varepsilon \leqslant 1.0$ and by curves of constant velocity for $\varepsilon \geqslant 5$.

Fig. 17. Stopping-power curves as a function of residual range for various ions in lead as calculated by the computer program. Various ion specific energies in units of MeV/amu are designated on each curve by symbols for $\varepsilon \leqslant 1.0$ and by curves of constant velocity for $\varepsilon \geqslant 5$.

Fig. 18. Stopping-power curves as a function of residual range for various ions in uranium as calculated by the computer program. Various ion specific energies in units of MeV/amu are designated on each curve by symbols for $\varepsilon \leqslant 1.0$ and by curves of constant velocity for $\varepsilon \geqslant 5$.

Fig. 19. Energy-range curves for various ions in water as calculated by the computer program. For any specific energy on the ordinate, the residual path-length range is read from the abscissa. At the left of the figure values of $\beta = V/c$ are displayed.

Fig. 20. Energy-range curves for various ions in aluminum as calculated by the computer program. For any specific energy on the ordinate, the residual path-length range is read from the abscissa. At the left of the figure values of $\beta = V/c$ are displayed.

Fig. 21. Energy-range curves for various ions in copper as calculated by the computer program. For any specific energy on the ordinate, the residual path-length range is read from the abscissa. At the left of the figure values of $\beta = V/c$ are displayed.

Fig. 22. Energy-range curves for various ions in silver as calculated by the computer program. For any specific energy on the ordinate, the residual path-length range is read from the abscissa. At the left of the figure values of $\beta = V/c$ are displayed.

Fig. 23. Energy-range curves for various ions in lead as calculated by the computer program. For any specific energy on the ordinate, the residual path-length range is read from the abscissa. At the left of the figure values of $\beta = V/c$ are displayed.

Fig. 24. Energy-range curves for various ions in uranium as calculated by the computer program. For any specific energy on the ordinate, the residual path-length range is read from the abscissa. At the left of the figure values of $\beta = V/c$ are displayed.

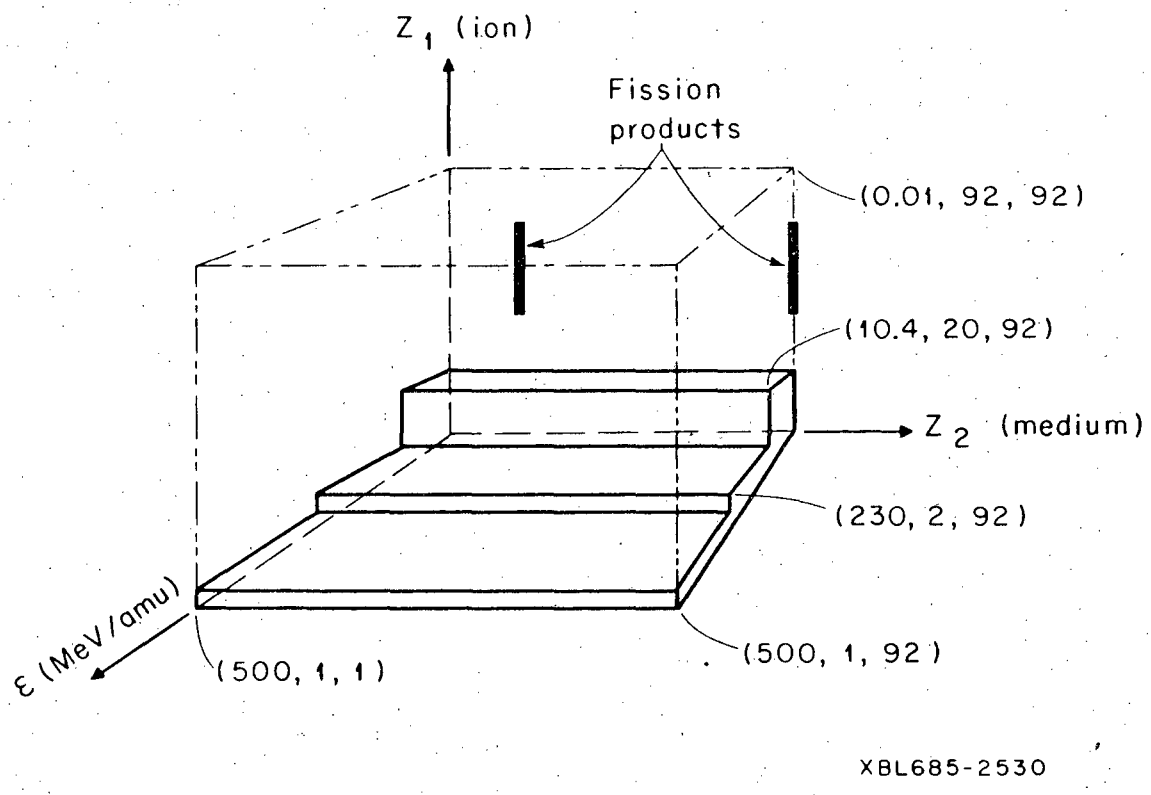
Z 1 (ion)
Fission products
(0.01, 92, 92)
(10.4, 20, 92)
Z 2 (medium)
(230, 2, 92)
ε (MeV/amu)
(500, 1, 1)
(500, 1, 92)
XBL685-2530

Figure 1.

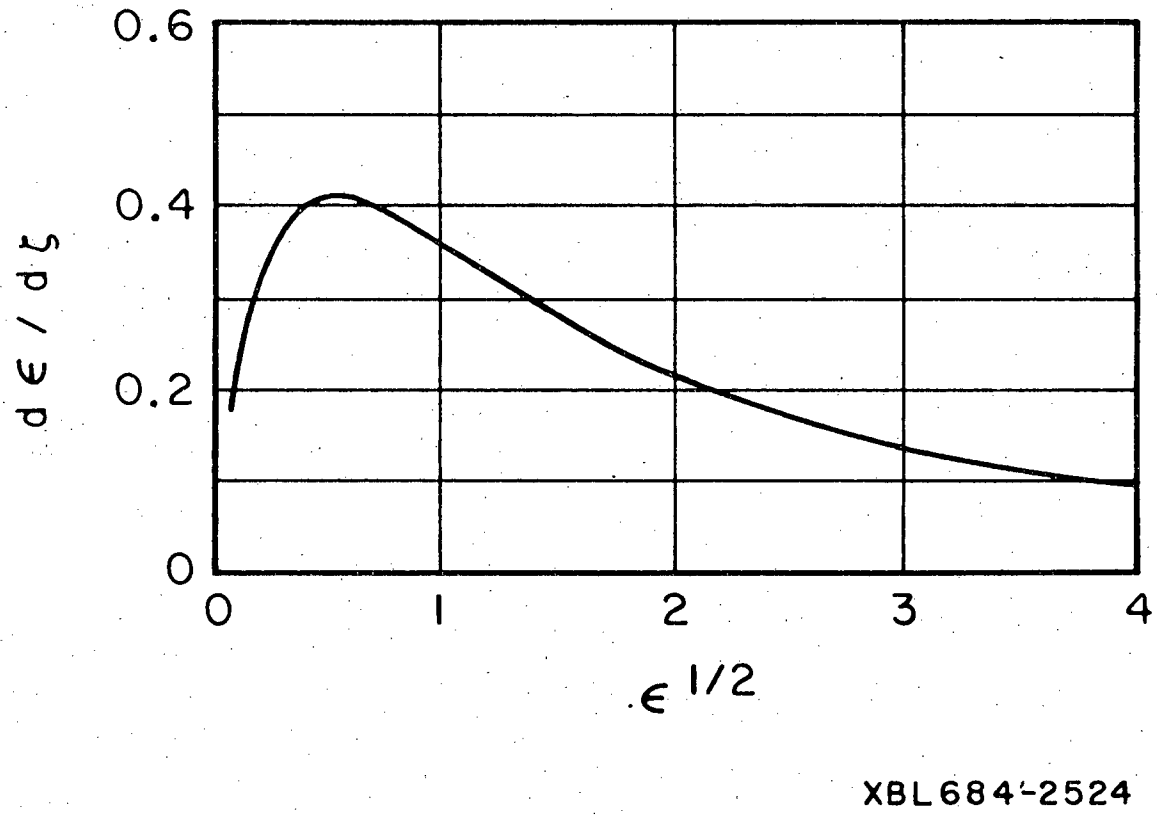


Figure 2.

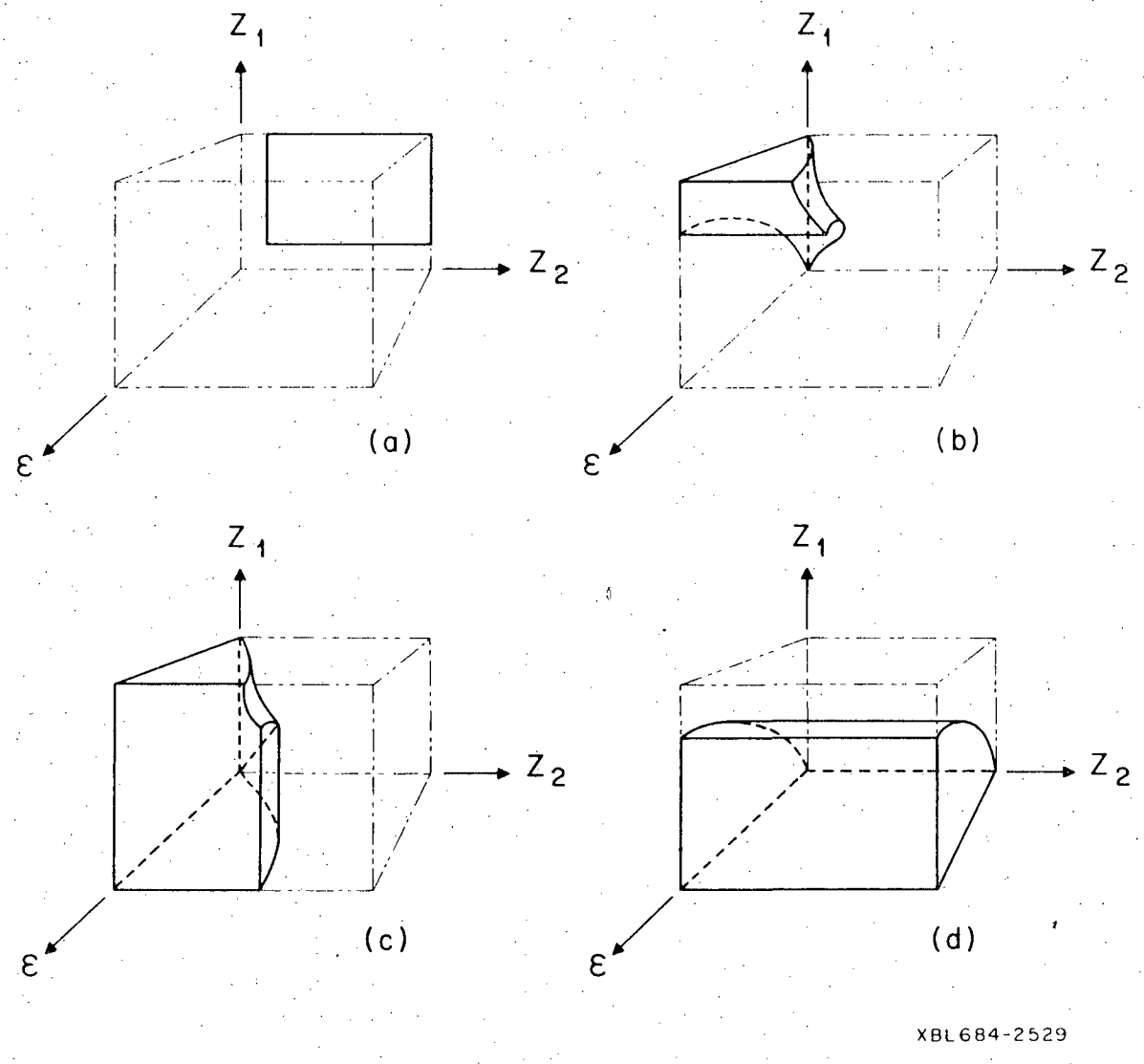


Figure 3.

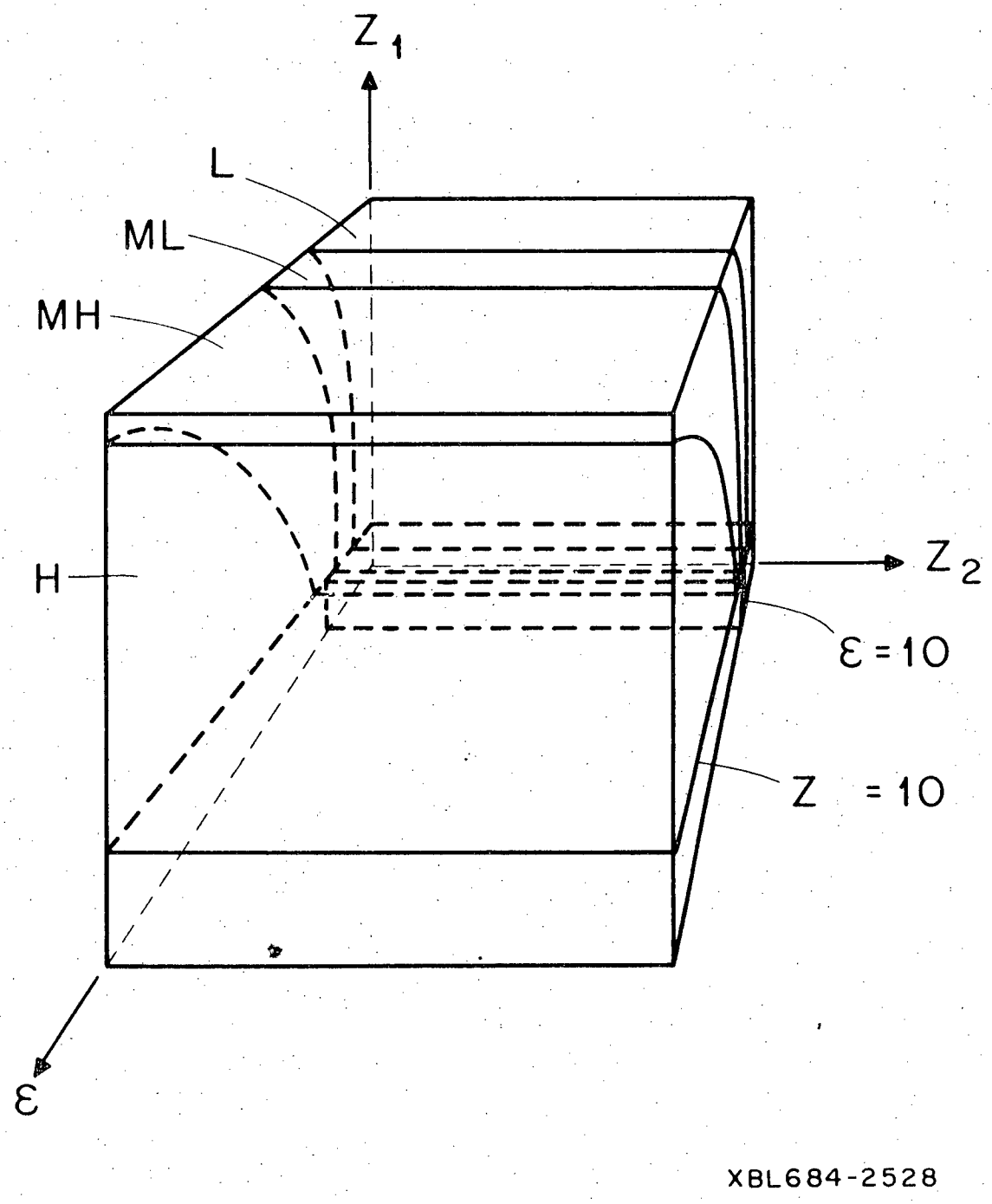


Figure 4.

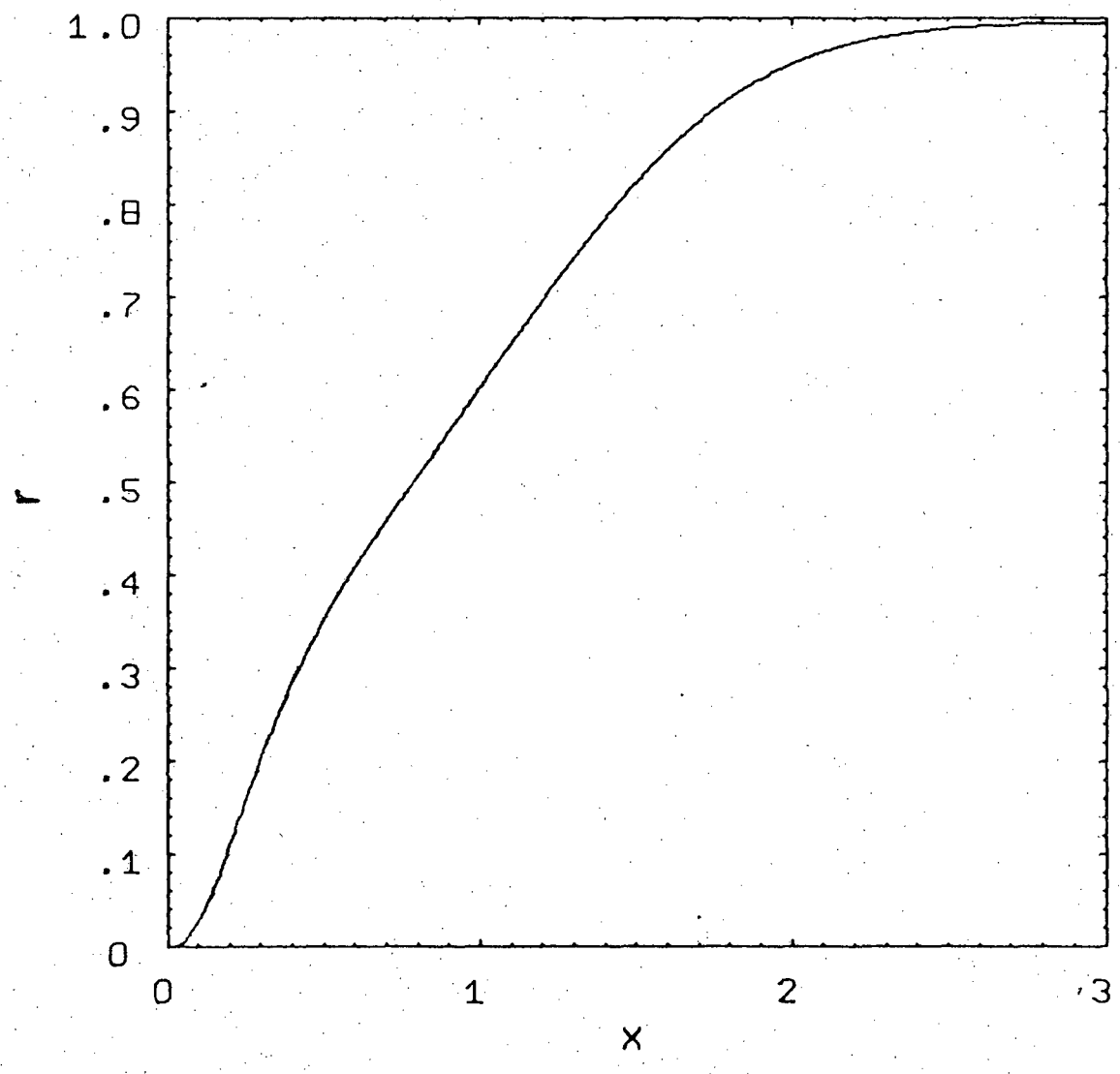


XBL 685-847

Figure 5.

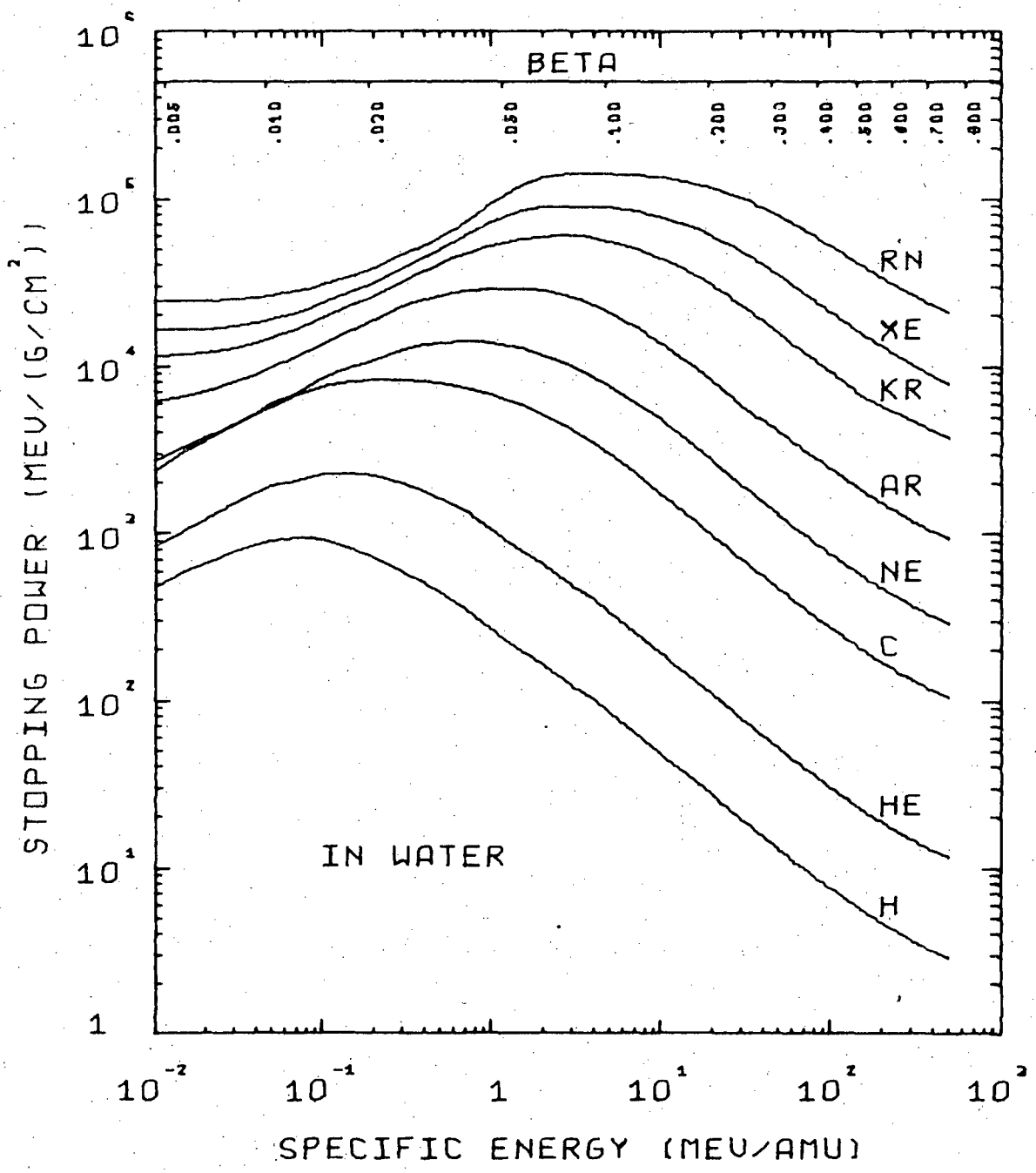


XBL 685-840

Figure 6.

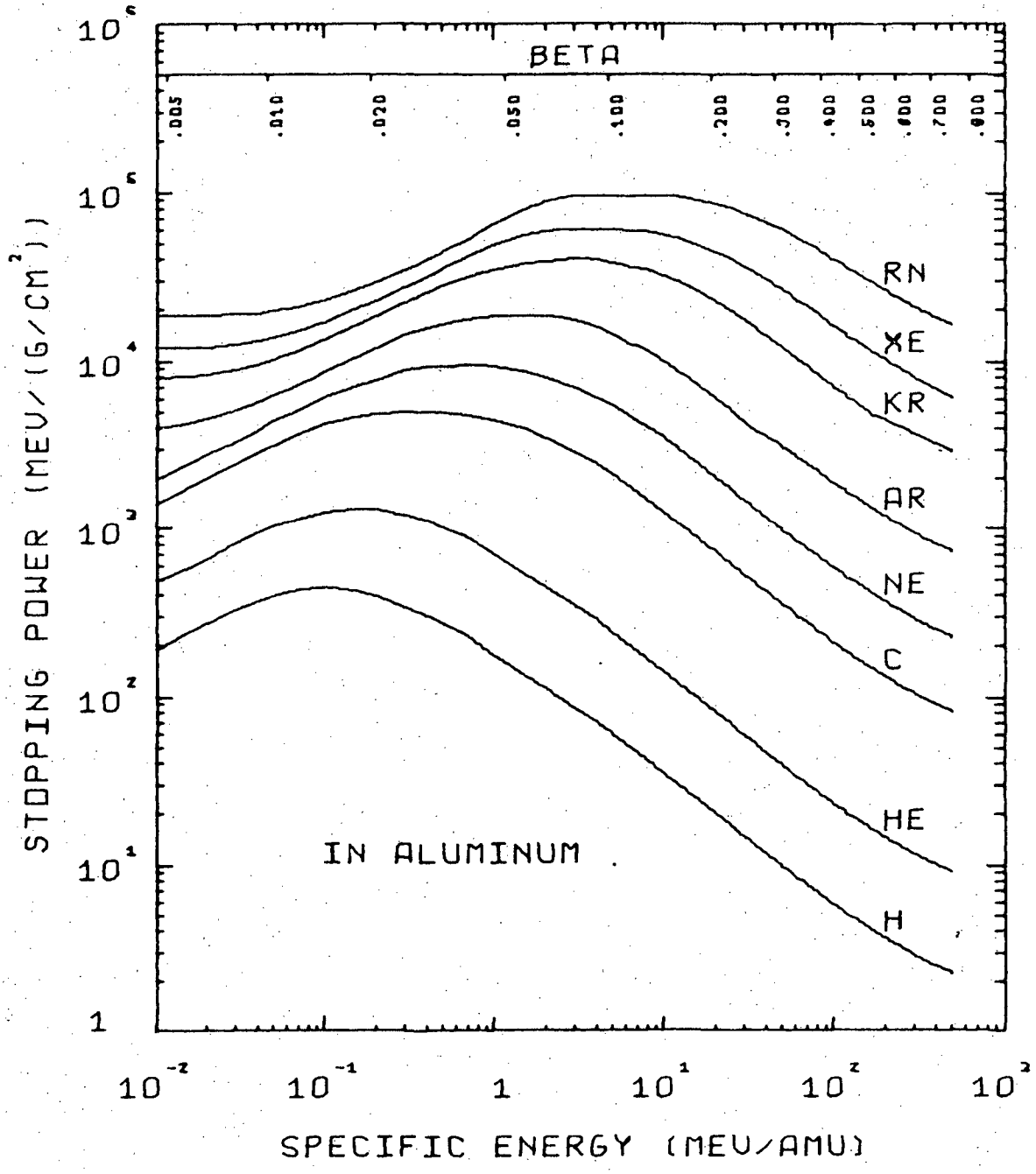


XBL 685-841

Figure 7.

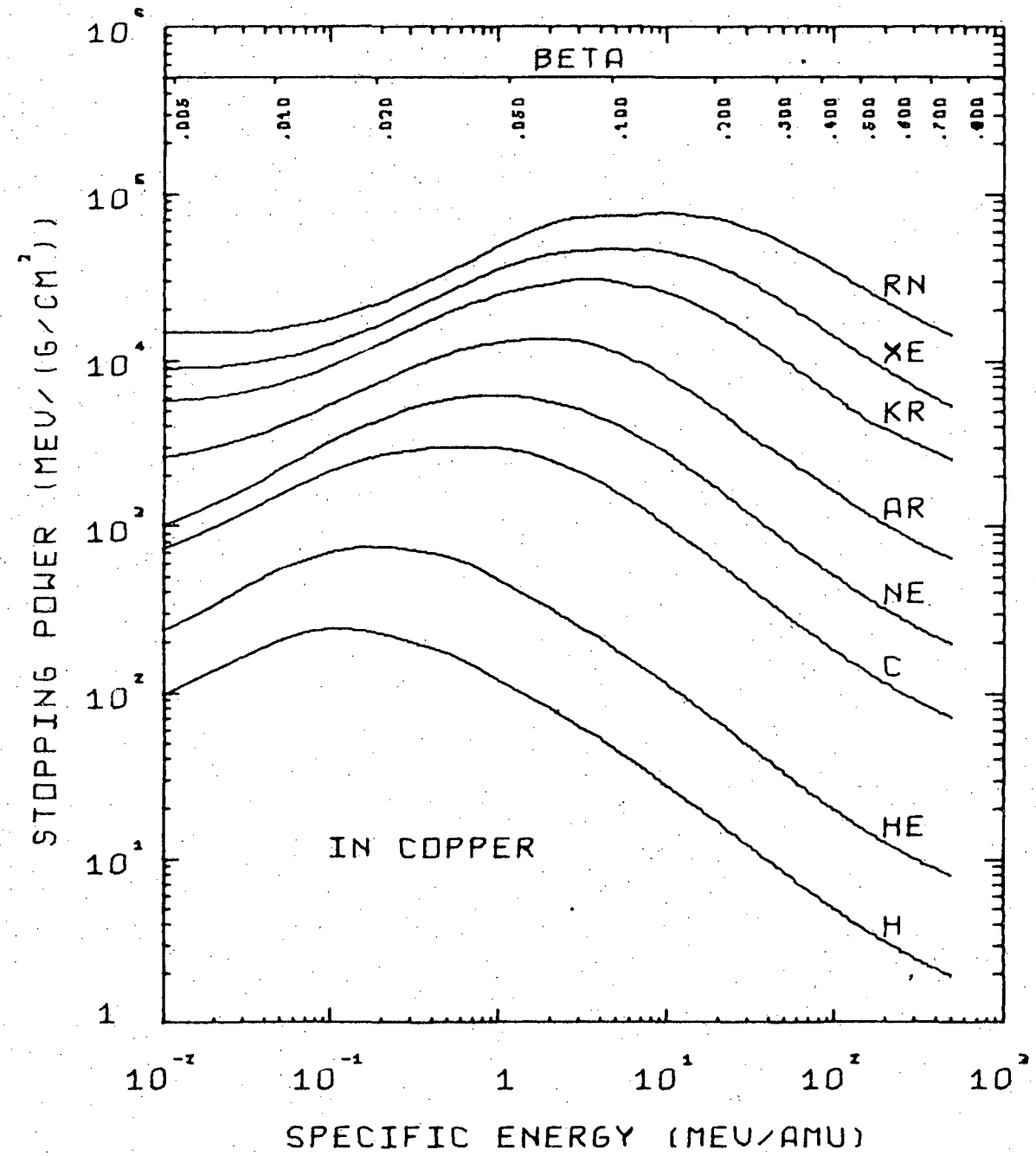


XBL 685-842

Figure 8.

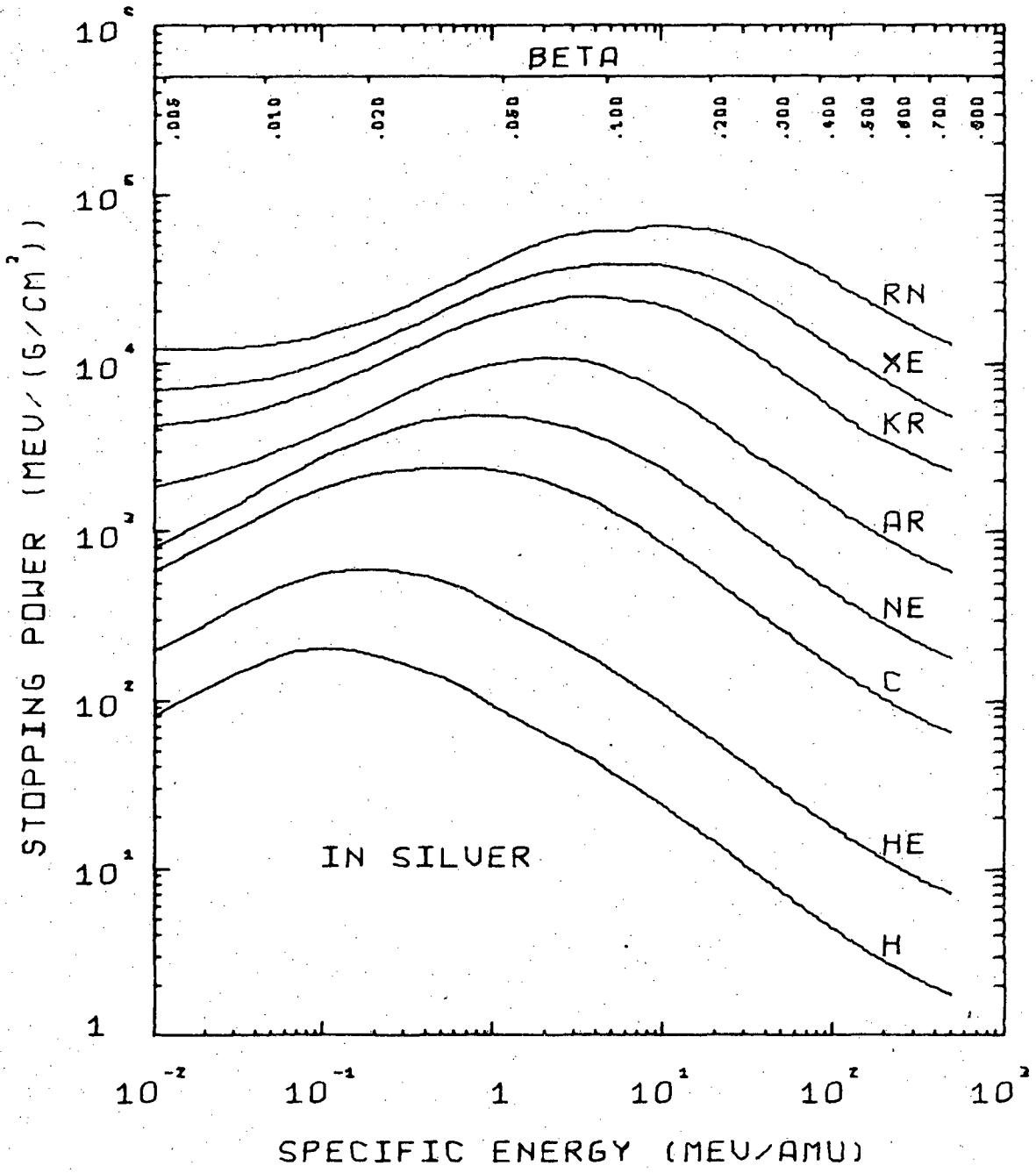


XBL 685-843

Figure 9.

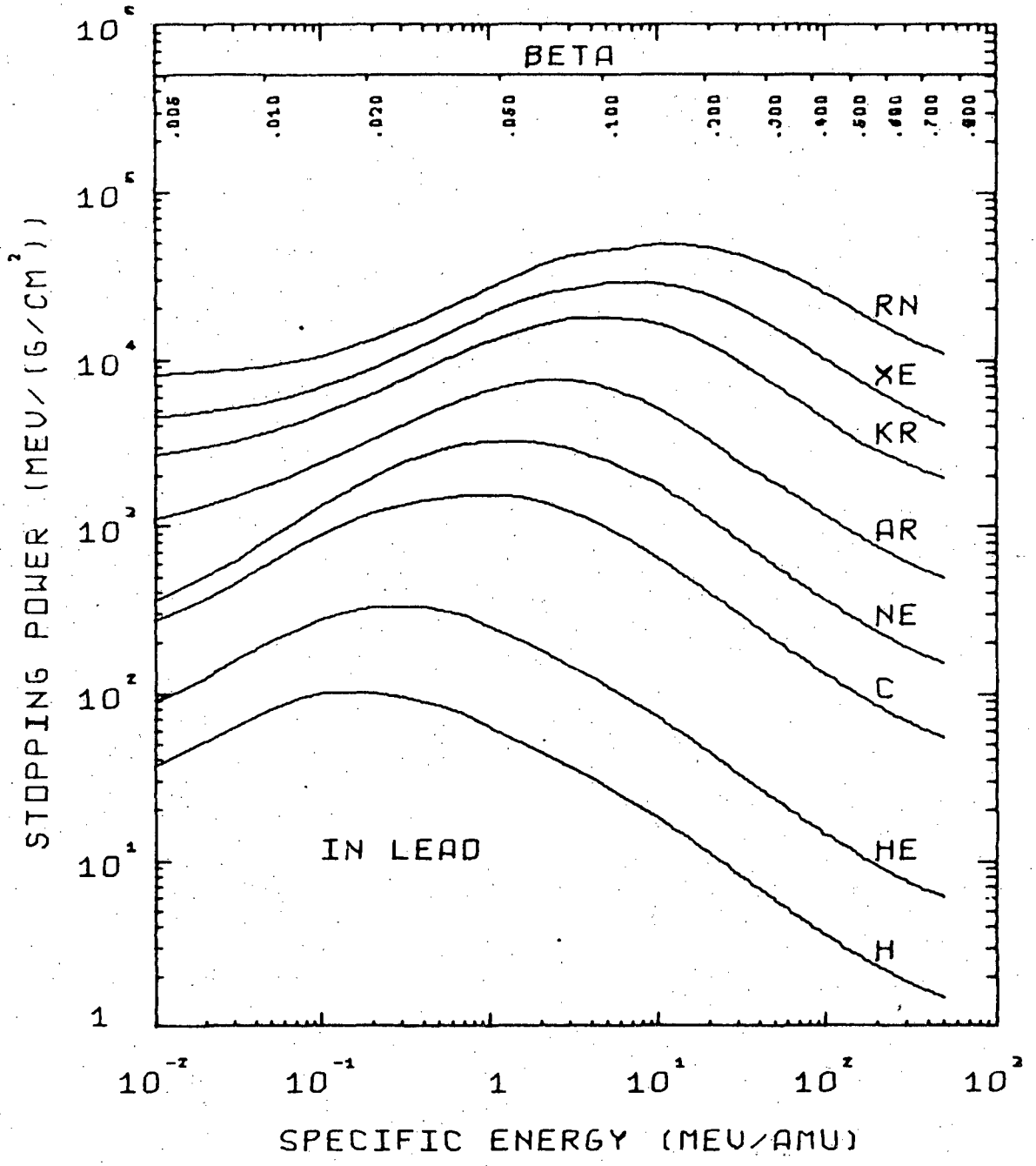


XBL 685-844

Figure 10.

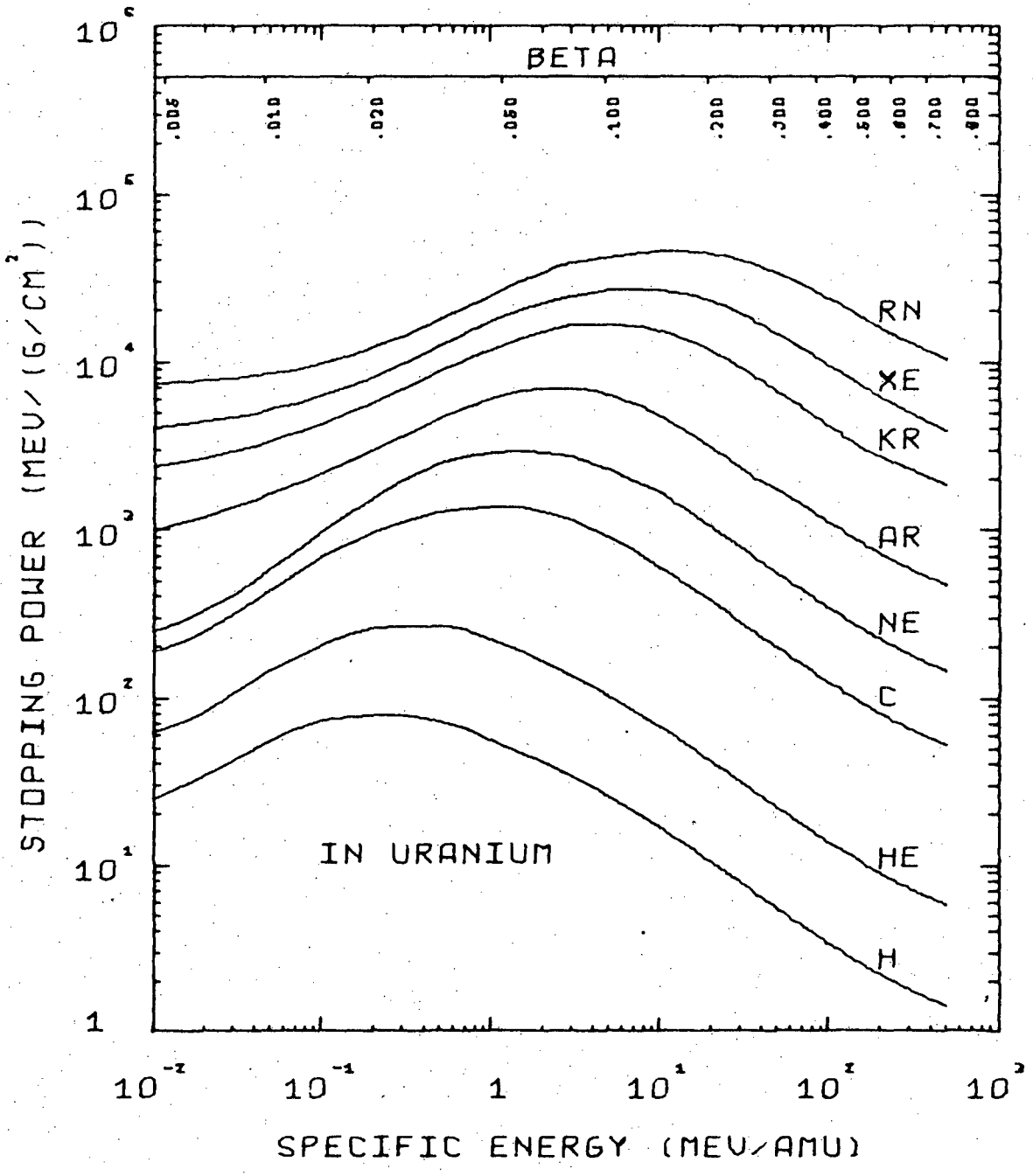


XBL 685-845

Figure 11.

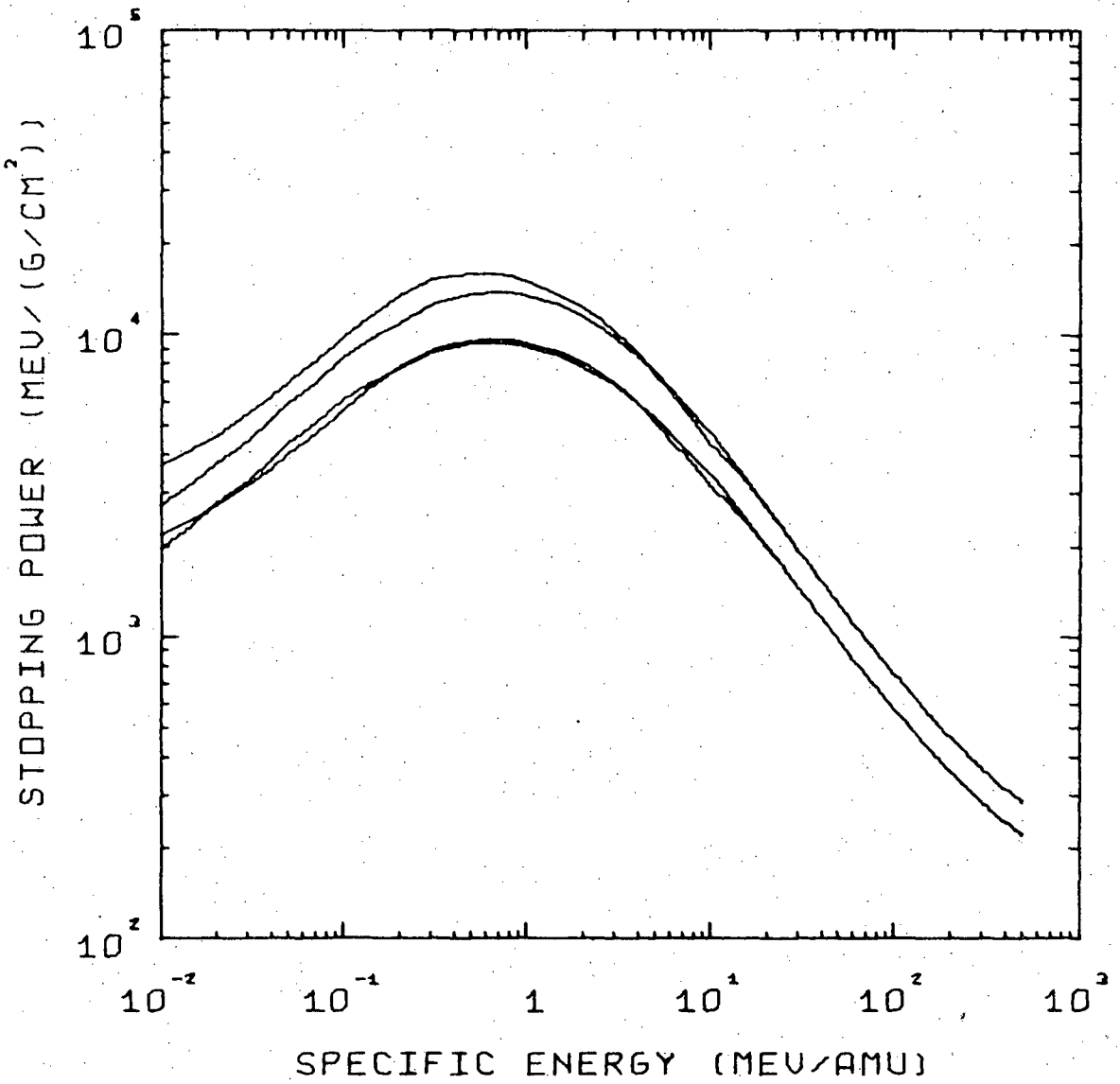


XBL 685-846

Figure 12.

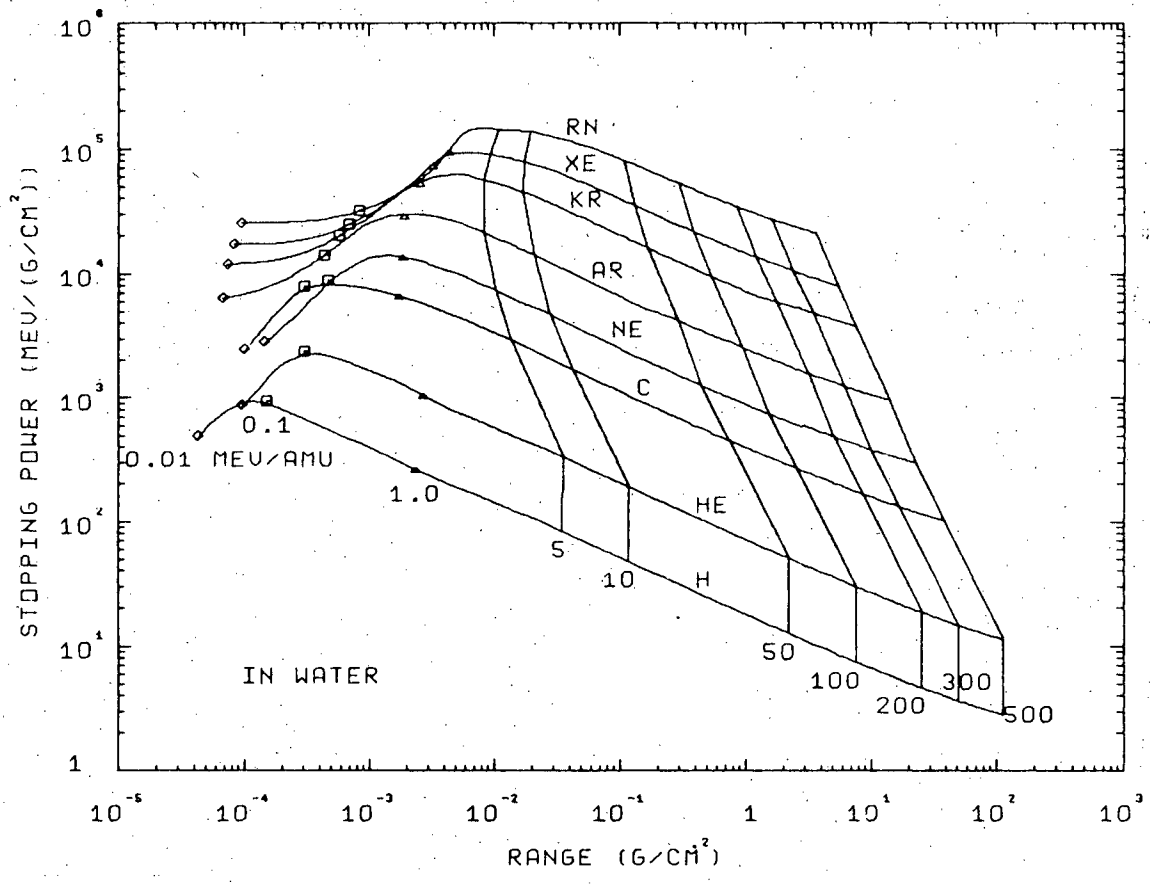
STOPPING POWER (MEV/(G/CM²))
RANGE (G/CM²)
RN
XE
KR
AR
NE
C
HE
H
0.01 MEV/AMU
0.1
1.0
5
10
50
100
200
300
500
IN WATER
XBL 685-827

Figure 13.

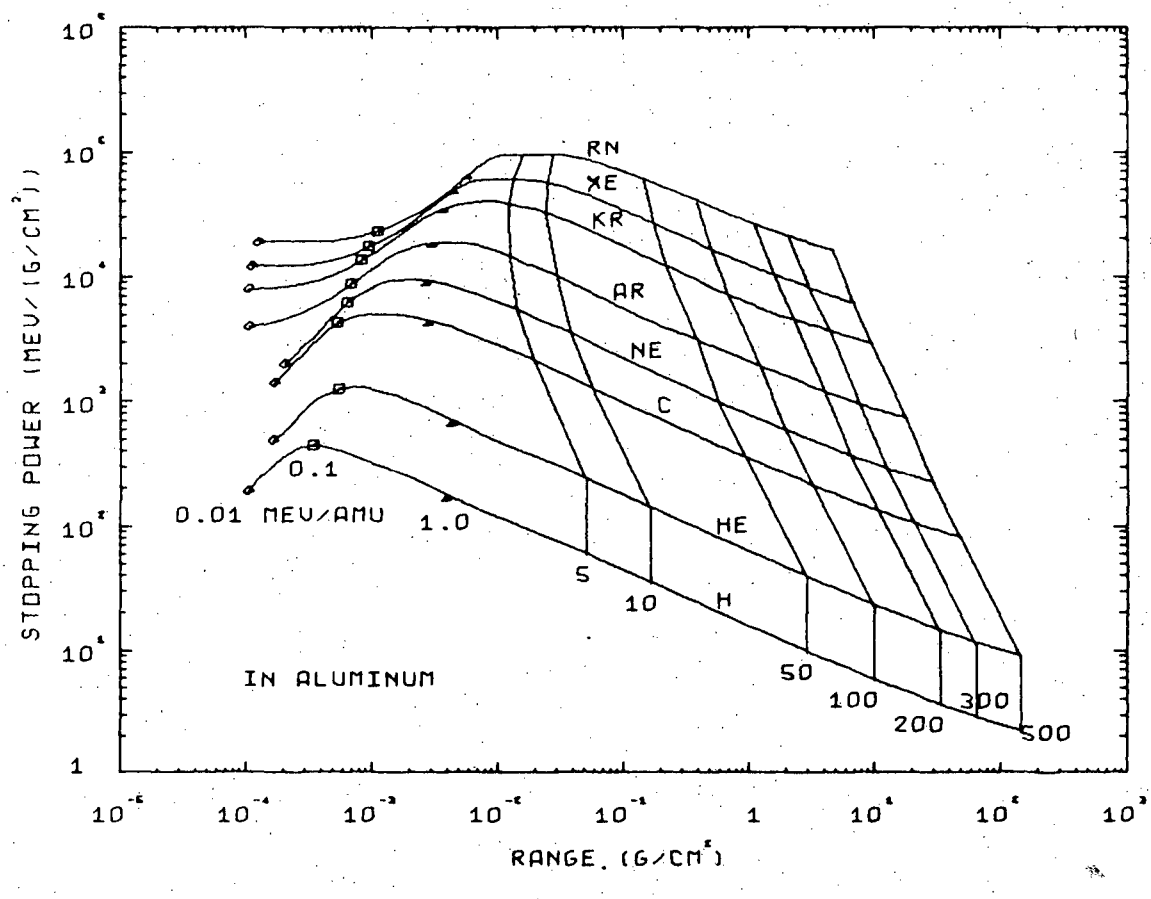


XBL 685-828

Figure 14.

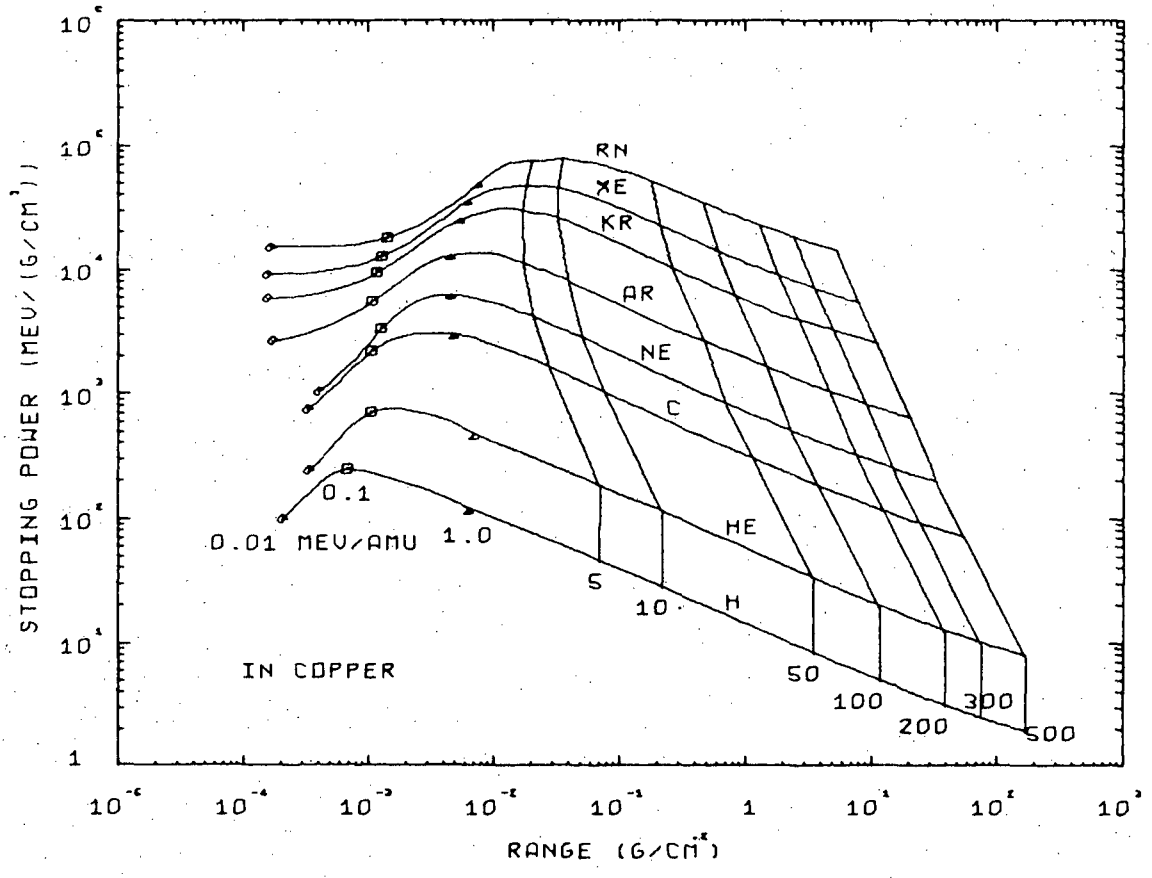


XBL 685-829

Figure 15.

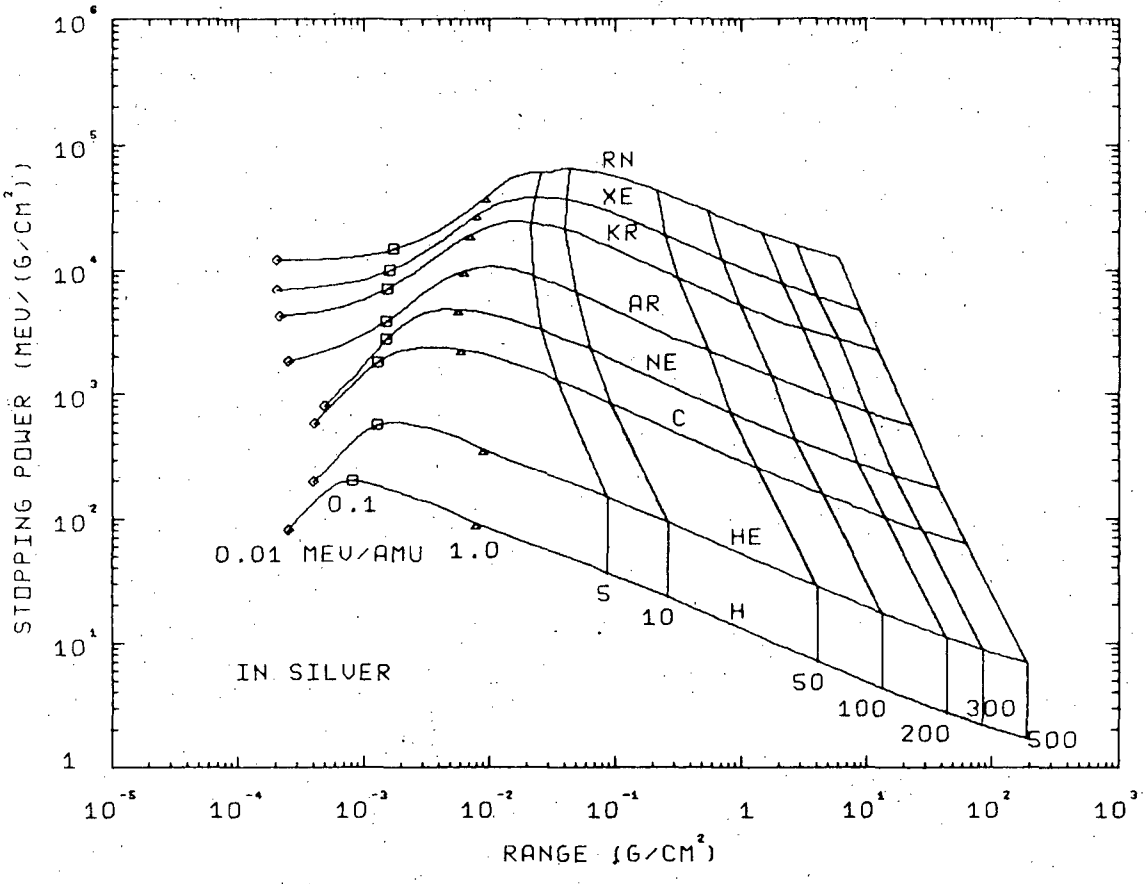


XBL 685-830

Figure 16.

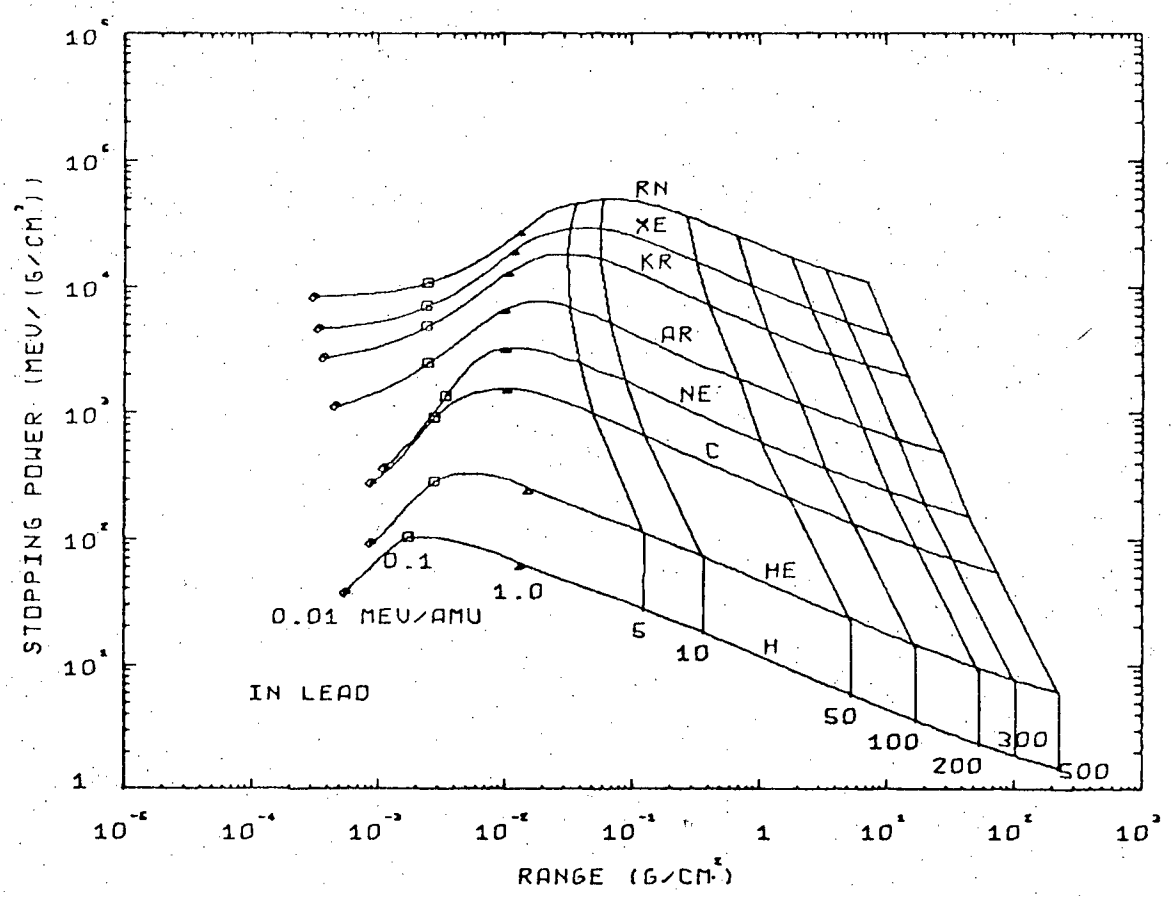


XBL 685-831

Figure 17.

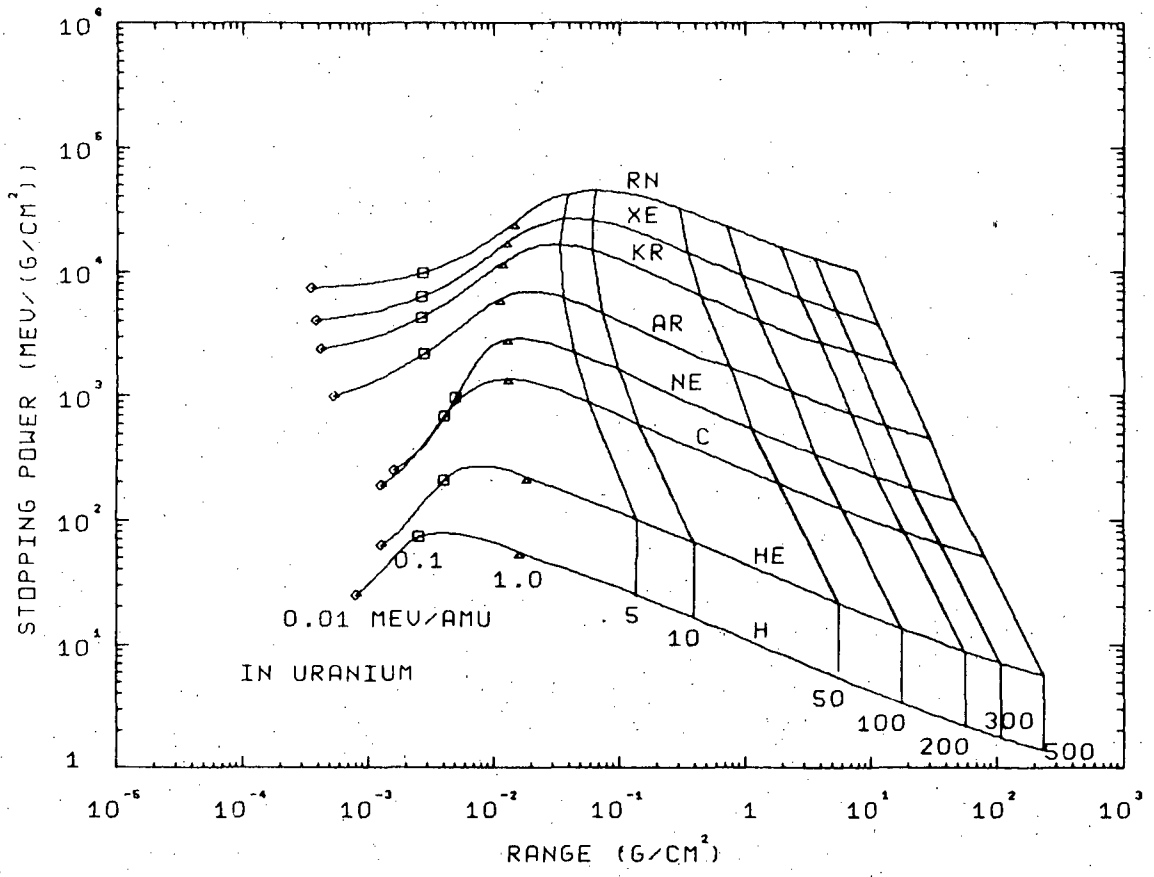


XBL 685-832

Figure 18.

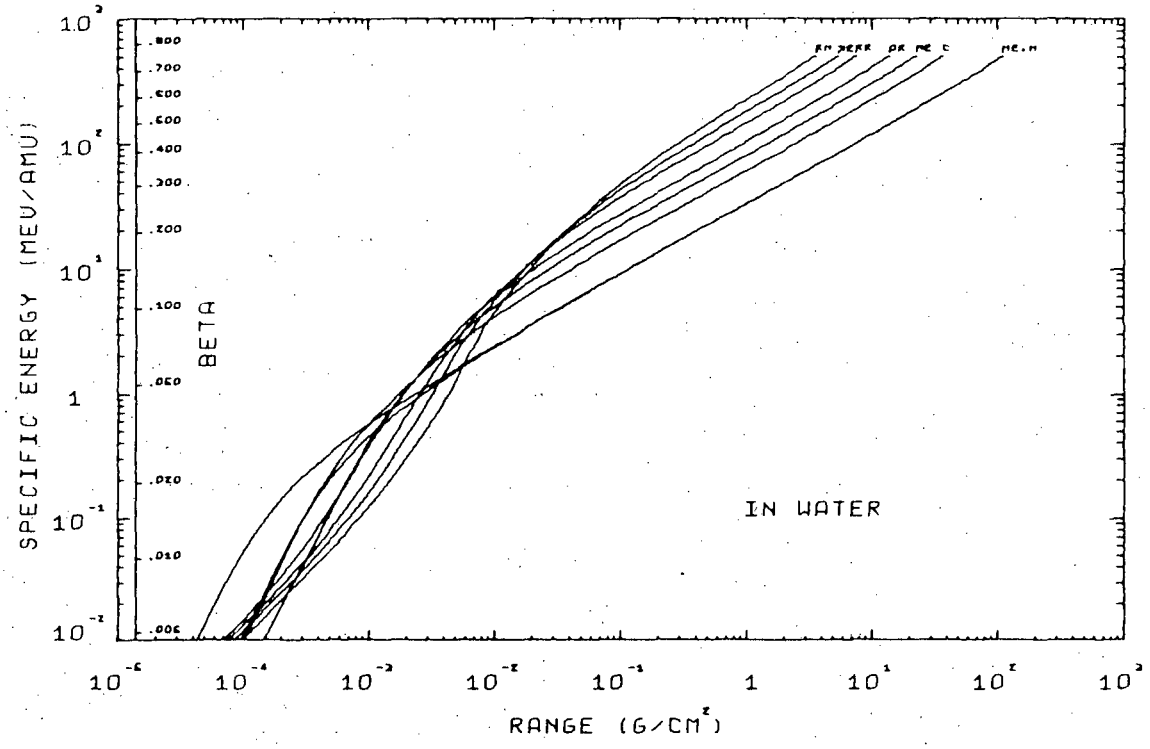


XBL 685-833

Figure 19.

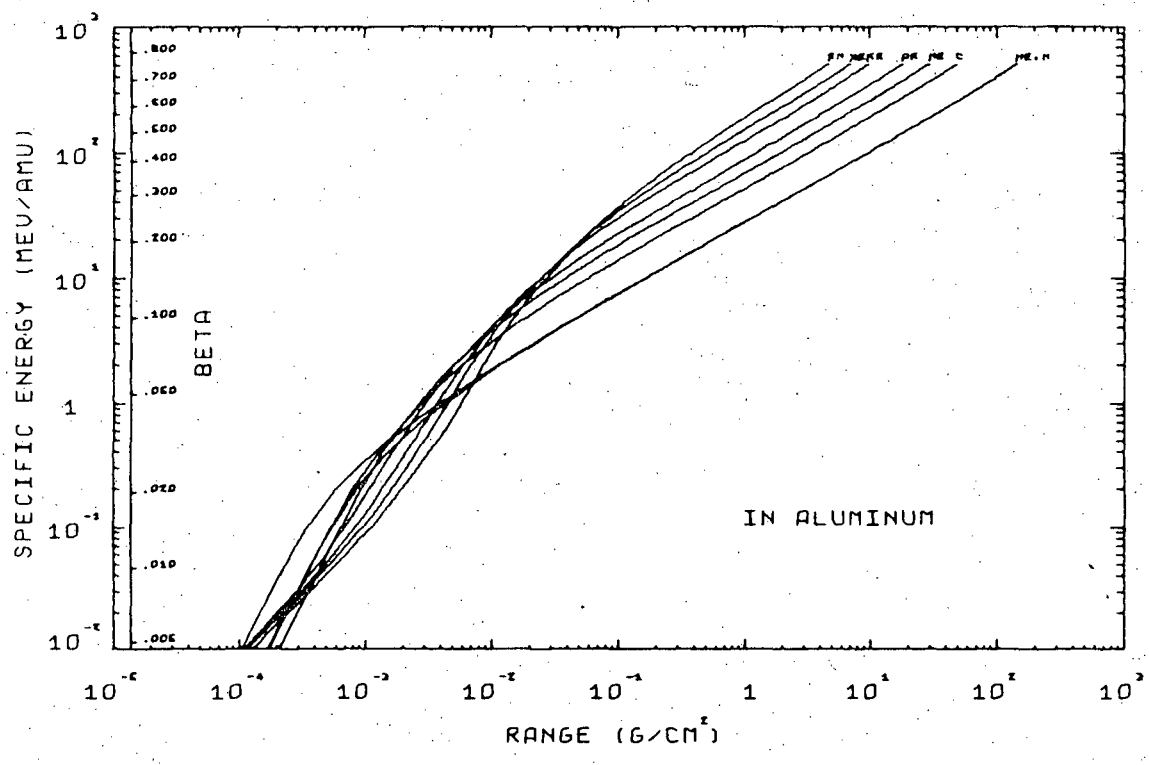


XBL 685-834

Figure 20.

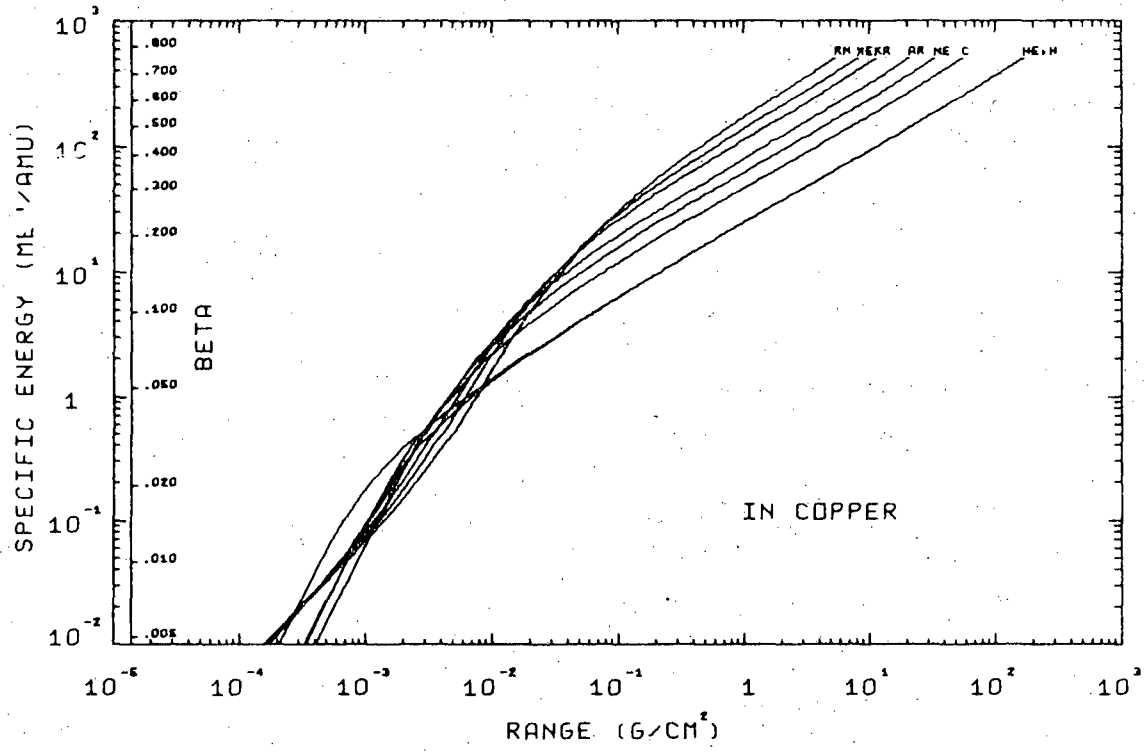


XBL 685-835

Figure 21.

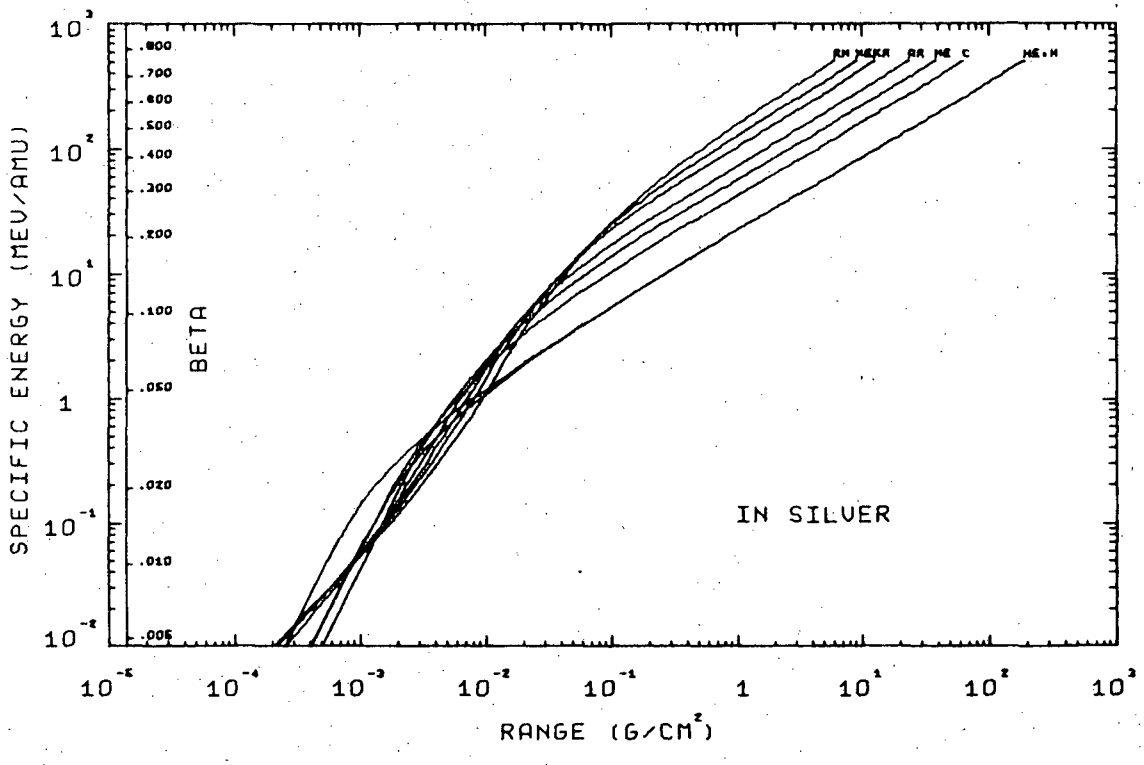
SPECIFIC ENERGY (MEV/AMU)
BETA
RANGE (G/CM²)
IN SILVER
XBL 685-836

Figure 22.

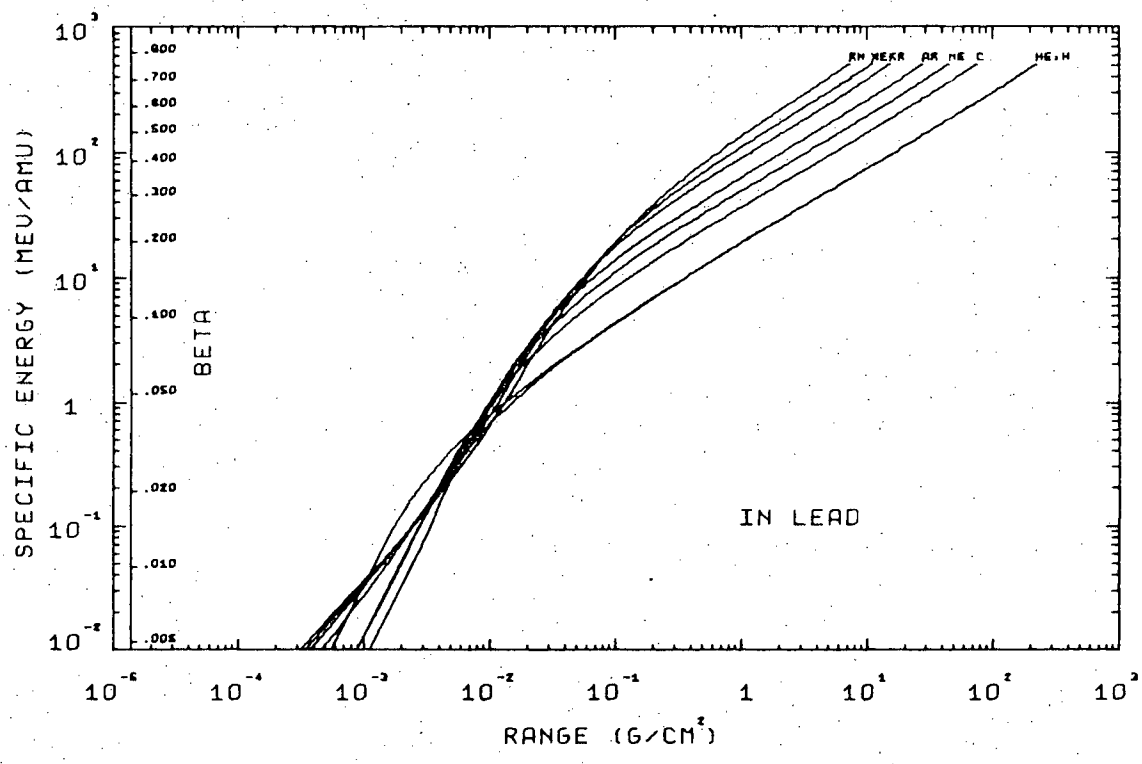


XBL 685-837

Figure 23.

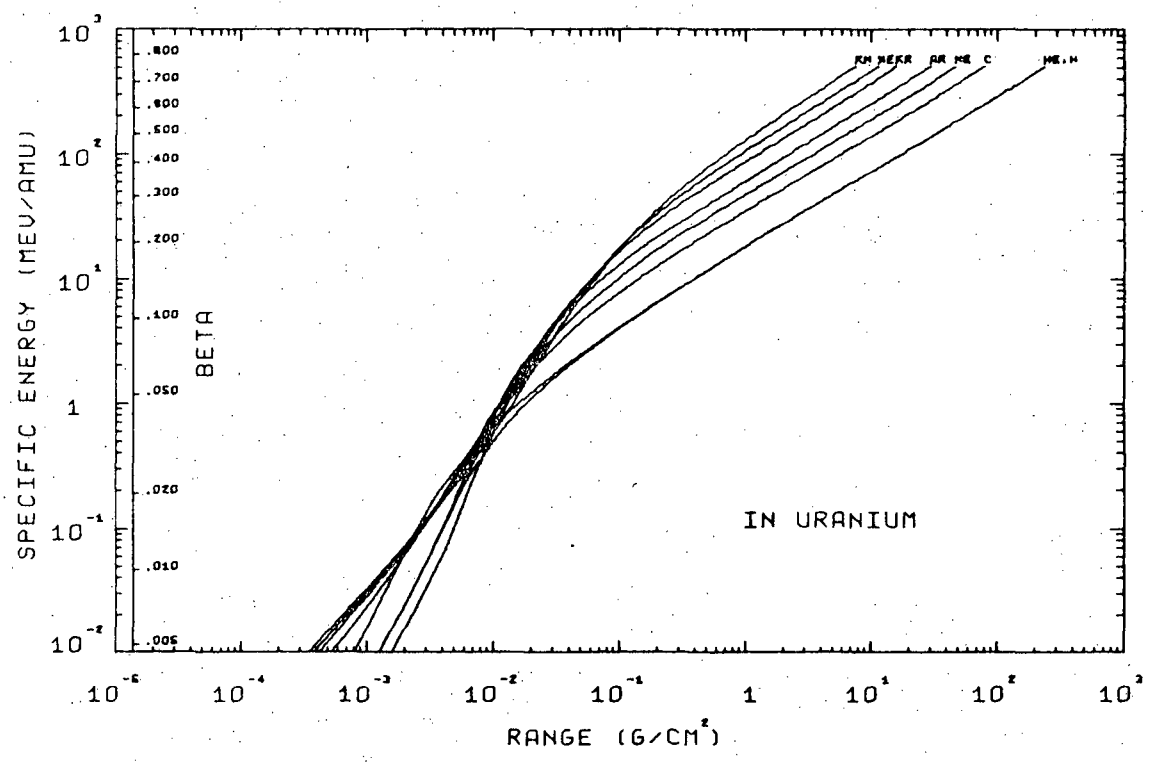


XBL 685-838

Figure 24.